dynardo
dynamic software & engineering

01/2014

Title Story // Master of Design – RDO with optiSLang
Increasing the efficiency of a steam turbine
Optimization of surgical fracture treatment
Model-based simulations of surgical procedures
Simulation, optimization and testing – successfully combined

RDO-JOURNAL

optiSLang
multiPlas
ETK
SoS

MASTER OF DESIGN – RDO WITH OPTISLANG

Within the virtual prototyping process, it is not always possible to reduce the complexity of the physical models to obtain an efficient calculation effort. Although, there has been progress in numerical methods and High Performance Computing (HPC), in such cases, to explore model configurations for Robust Design Optimization (RDO) is impracticable. Therefore, efficient surrogate models are required.

With the Metamodel of Optimal Prognosis (MOP), optiSLang provides an automatic approach for the selection of optimally suitable meta-models in regard to the optimization task. It represents the best compromise between available sample information and the model representation in terms of considered input variation. This determination is supported by optiSLang's Coefficient of Prognosis (CoP) serving as an objective and model independent quality measure. Thus, combined with an automatic reduction of the variable space by using advanced filter techniques, an extensive optimization potential can be explored to master even high dimensional tasks. optiSLang enables the engineer to use this approach in an automated mode. Therefore, the RDO-modules of a sensitivity analysis, optimization and robustness evaluation can be implemented in daily virtual product development.

During the conduction of a sensitivity analysis, optiSLang's MOP/CoP procedures identify the variables which contribute most to a certain optimization goal. Additionally, this procedure helps the engineer to appropriately formulate the optimization task and to predict the results of the numerical CAE solver. This approach leads to a minimization of necessary solver runs.

In the optimization module, a Best Practise Management provides a wizard supported selection of the most efficient optimization strategy and the best fitting algorithms.

During the following robustness evaluation, optiSLang measures the variation of important response values as a result of scattering inputs and quantifies the robustness of the design. With the help of the CoP, the contribution of the different sources of input variation towards the response variation will be indicated. In case of response scatter violating the limits, responsible input scatter can be reduced. As a result, the design will be modified in a way to minimize response scatter or to move response scatter within given bounds.

optiSLang's drag and drop modules of sensitivity analyses, optimization and robustness evaluation as well as the Best Practise Management additionally, simplify the definition of parameter ranges, objectives and constraints and minimize the necessary user input.

In the title story of this issue, an application is explained to illustrate the benefits of using optiSLang and how to become a master of CAE-based Robust Design Optimization.

Apart from that, we again have selected case studies about CAE-based RDO from different industries. I hope you will enjoy reading our magazine.

Yours sincerely

Johannes Will
Managing Director DYNARDO GmbH

Weimar, May 2014

CONTENT

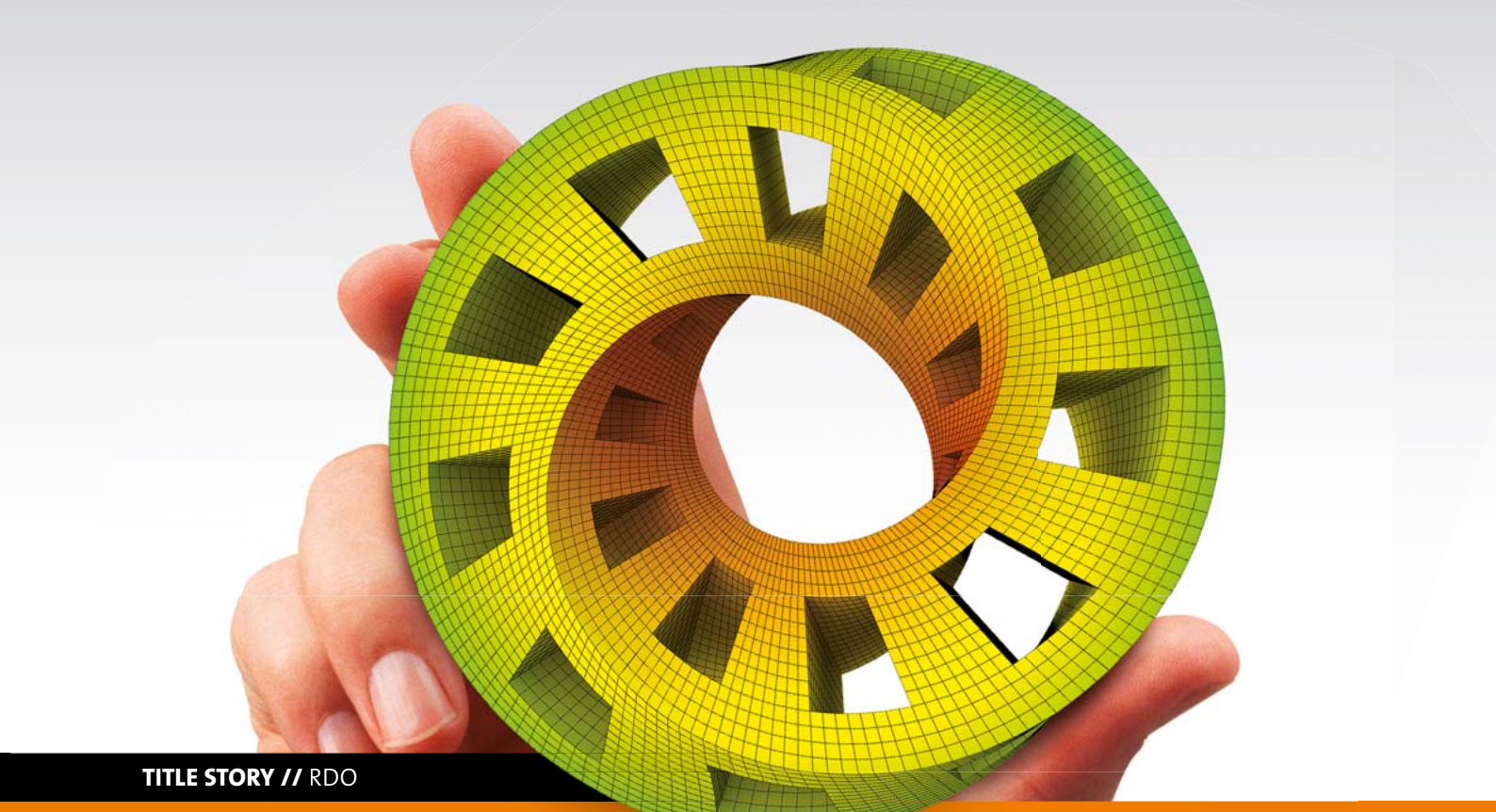

MASTER OF DESIGN – CAE-BASED ROBUST DESIGN OPTIMIZATION WITH OPTISLANG

Sensitivity analysis, optimization and robustness evaluation with a minimum amount of user input and solver runs for your effective virtual product development.

optiSLang as algorithmic toolbox for RDO

In the field of product engineering, the introduction of technical innovations as well as the requirements for improvement of product performance are accelerating and increasing. Thus, product life cycles and development times are constantly getting shorter. Therefore, there is a high demand for virtual product development (Computer Aided Engineering, CAE) and CAE-based optimization tools. At the same time, quality requirements of reliability and robustness are increasing. Robust and optimized product designs are needed. Considering this, CAE-based Robust Design Optimization (RDO) becomes more and more important. To address these challenges, optiSLang offers you an algorithmic toolbox to meet all requirements.

With optiSLang you are able to:

- couple any (CAE) solver software to your workflow and use it for automation of your process chain
- manage an unlimited number of parameters due to automatic input reduction
- handle design failure up to 50%, non-linear CAE-problems and noisy responses
- standardize your process for quality assurance
- perform variant studies, sensitivity analysis, optimization, robustness and reliability evaluation within a single workflow

The general RDO methodology which will be discussed in this article is the following:

1. Sensitivity analysis to focus on important inputs
2. Deterministic optimization to find the optimal design
3. Robustness evaluation to evaluate input tolerances of the best design by stochastic methods

Parametric modeling, process integration and automation

To solve RDO tasks, the availability or generation of a suitable (CAE) parametric model is a key requirement. Parametric modelling environments like ANSYS are very powerful and can be easily integrated with optiSLang. Even a full integration of optiSLang into ANSYS Workbench is available. In principle, any other solver can be easily coupled to optiSLang. We offer you a great variety of supported integrations which includes, amongst others:

- any solver that can be executed in batch-mode handling ASCII-input and -output files
- ANSYS Workbench and ANSYS classic
- Abaqus
- FloEFD
- AMESim and Simulation X
- Python, Matlab and Excel

After your process is integrated, it can be automated and used as standardized process. The process chain can be expanded by additional solvers or pre- and post-processing tools within a single workflow. For any time- or frequency-dependent RDO task, optiSLang's functionality of signal processing significantly helps to extract particular responses out of signal data.

Best practice modules

One of the main innovations of optiSLang v4 is the availability of best practice workflow modules with wizard guidance to choose the most appropriate algorithms with robust default settings. With the help of the following three modules:

- **Sensitivity analysis** to understand the design, to reduce the input parameter space to the most important inputs, to check the prediction quality of response variation and to automatically generate the optimal meta model
- **Optimization** to improve design performance
- **Robustness evaluation** to check design robustness exposed to scattering material parameters, production tolerances or scattering environmental conditions

The user input is minimized to define the parameter ranges and their scattering, as well as objectives and constraints. All modules can be applied via drag and drop into the scenery of the project page.

Focus on important design parameters

As a first step before the actual optimization procedure, it is always recommended to perform a sensitivity analysis. With this analysis, you can study how the output variation is affected by different sources of input variation and thus, to reduce the input parameter space for the RDO task.

The most relevant methodologies for a global sensitivity analysis implemented in optiSLang are:

1. Scanning the input parameter space with advanced Latin Hypercube Sampling to avoid clustering and to cover optimally the input parameter space.
2. Identification of the most important input parameters and quantification of their contribution to response variation using optiSLang's **Metamodel of Optimal Prognosis (MOP)** algorithm and variance based sensitivity analysis.

The main benefits of optiSLang's sensitivity analysis are:

- Automatic identification of the MOP with maximal prognosis quality by determination of best approximation model (e.g. polynomial, Moving Least Squares) for each output in the optimal subspace of important input parameters
- Automatic reduction of inputs of those being important to describe the output variation
- Assessment of the prediction quality of the MOP by optiSLang's **Coefficient of Prognosis (CoP)** including quantification of input importance
- Quantification of numerical noise of the outputs
- Estimation of the optimization potential: are the chosen input parameters in the right range to achieve the objective? Are objectives conflicting? Can the MOP be used to approximate the solver output for further optimization?

Design optimization

Within the optimization framework, several algorithms for single and multi-objective optimization are available:

- Gradient-based methods
- Adaptive Response Surface Method
- Nature inspired algorithms such as evolutionary algorithms or particle swarm optimization

The choice of the most suitable and efficient optimization method is automatically provided by optiSLang workflow wizards. This choice is based on the results of the sensitivity analysis and the optional user-defined input, like the number of objectives, parameters and failed designs as well as the level of solver noise.

There are two main optimization strategies:

1. The search of the best design is performed on the MOP as a very efficient pre-search without any additional solver calls. Then, the best design of the MOP can be used as the final design after validation with a single solver call or as a start design for a subsequent optimization
2. Standard optimization with direct solver calls using the reduced input parameter set of the sensitivity analysis

Evaluate tolerances

To match quality requirements of designs exposed to given material and environmental variations or geometry tolerances, their scatter of all important responses needs to stay within acceptable ranges. To prove that, a variance based robustness evaluation can be performed.

In this context, the first step is the assignment of scattering input parameters by definition of their scatter range, distribution and correlation among each other. Then, the robustness space is scanned by advanced sampling methods and the resulting response scatter is quantified. By using the MOP ap-

proach, we can additionally identify the most important scattering input prameters and quantify their importance.

Several strategies for robustness evaluation are possible to be realized in optiSLang:

1. Robustness evaluation after determination of the best design
2. Sequential optimization and robustness evaluation
3. Fully coupled robust design optimization

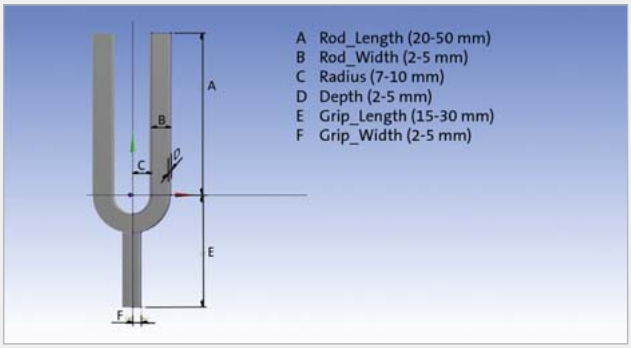

Fig. 1: Geometry input parameters of the tuning fork design

Example: Tuning Fork in ANSYS classic

Introduction

With the simple example of a tuning fork, the whole workflow will be presented comprising integration, sensitivity analysis, optimization and robustness evaluation in optiSLang. A modal analysis with a fixed support of the tuning fork and an undamped oscillation is performed within the parametric modeling environment ANSYS classic.

Integration

The integration is created via batch-script that executes ANSYS classic in batch mode and ASCII-input and –output files. This integration is fully supported in optiSLang and therefore very simple to generate.

Definition of input and output parameters

For the sensitivity analysis and optimization, six input parameters were considered. Namely, these are the geometry parameters rod length, rod width, grip length, grip width, radius and depth (Fig. 1). At the same time, four output parameters are evaluated: the frequencies obtained by the modal analysis (frequency 1, 2 and 3) and the mass.

Optimization task

The aim of the optimization was to equalize the main frequency 1 to 440 Hz and the higher frequencies to their duplicates and triplicates respectively. Thus, a single objective target optimization was performed by taking the quadratic deviation to the target value and by weighing the importance of the targets. The objective function which should be minimized is $(\text{frequency\_1-440})^2 + ((\text{frequency\_2-880})/2)^2 + ((\text{frequency\_3-1320})/4)^2$. As a constraint, the mass should be lower than 12 g.

Sensitivity analysis

As a pre-optimization step and for the identification of the most important inputs, a sensitivity analysis was performed. By obtaining an MOP for each output, an input parameter reduction is possible. Figure 2 (top) shows the CoP matrix as a result of this procedure. For instance, 98 % of frequency 1 can be explained by the MOP with only five inputs (rod width, rod length, grip width, grip length and depth) instead of six considered input parameters. The MOP for frequency 1 is illustrated in Figure 2 (bottom).

Optimization

After choosing the appropriate optimization algorithm by optiSLang's workflow wizard, the optimization can be performed based on the reduced input parameter set. First, a gradient-based optimization on the MOP with best design validation was chosen using predefined settings of the optimizer. 200 design points were evaluated until the algorithm was converging. In a second step, the best design of this MOP pre-search was used as a start design for an optimization with Adaptive Response Surface Method (ARSM) with direct solver calls. The search window of the start range for the ARSM was reduced to 10 % to generate a local search. The post-processing window of these results is illustrated in Figure 3.

The benefits of using optiSLang for this optimization are:

- The optimization was performed much faster: without the MOP, 200 solver calls would have been necessary for the first optimization step. This results in 33 minutes of time saved with calculation durations of 10 seconds per design.
- The properties of the best design were considerably improved. By comparing with the original design, the mass was reduced from 29.2 g to 9.9 g and the frequencies matched the target values (Figure 3). The starting values were 414, 417 and 959 Hz.

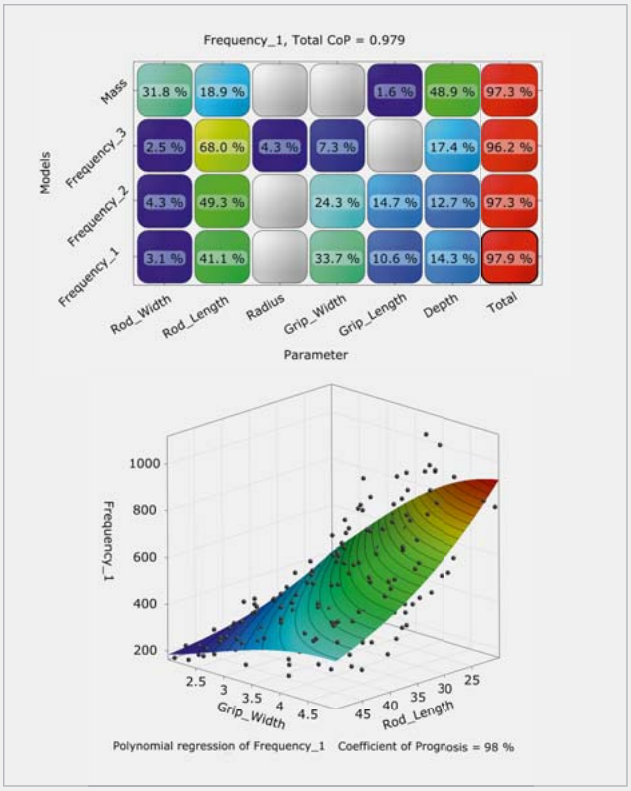

Fig. 2: Results of the sensitivity analysis: CoP matrix (top) / Metamodel of Optimal Prognosis for frequency 1 in dependence of the two most important inputs (bottom)

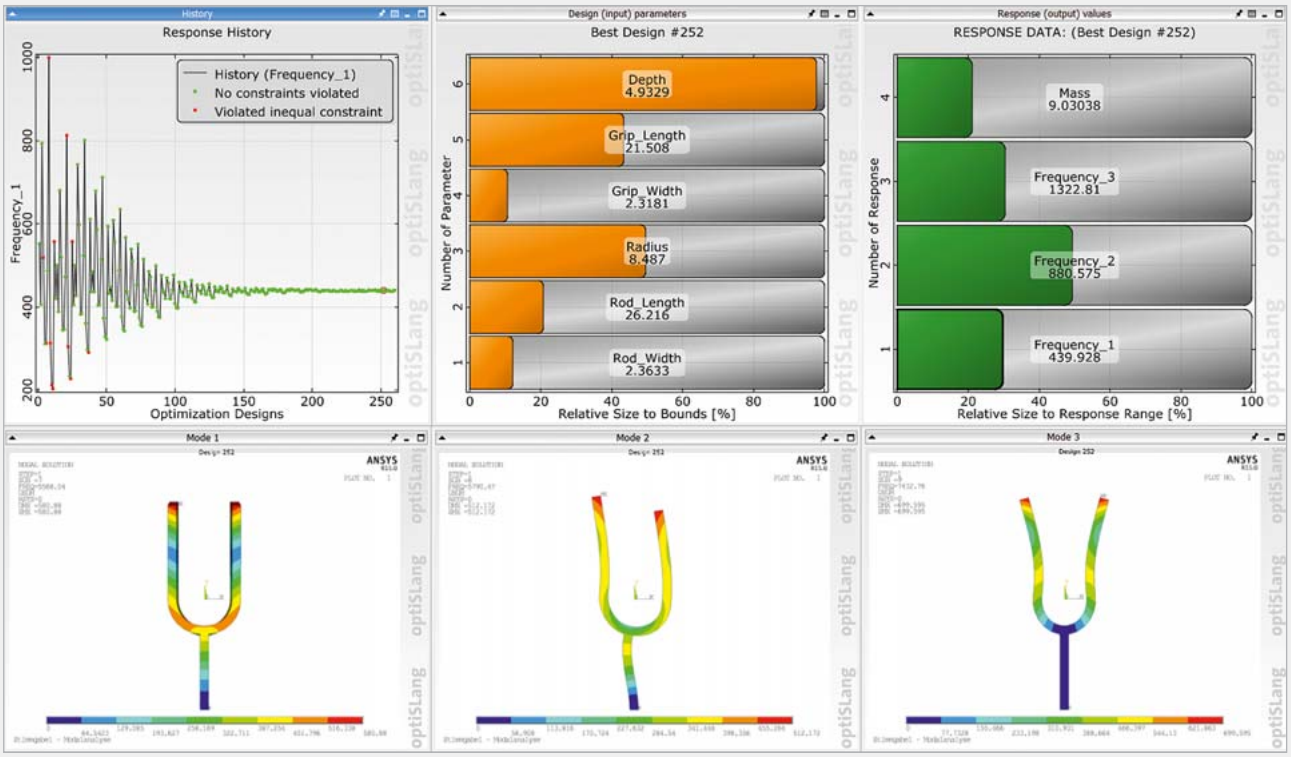

Fig. 3: Results of the optimization with Adaptive Response Surface Method: the response history shows the iterative convergence to the target value of 440 Hz. The input and output parameter values can be monitored. Furthermore, images of the modal frequencies were displayed for each design.

Robustness evaluation

For the robustness evaluation of the best design, besides geometry parameters, material parameter variations (here: E-module) were also considered in order to recognize critical inputs and to reduce uncertainties. All geometry parameters were varied with 0.5 % scatter relative to the mean and 1 % for the E-module with normal distribution respectively.

For a robust design, ± 7 Hz variation of the first frequency were defined to be acceptable. As a result of the robustness evaluation (Figure 4 (A)), 13 % of the designs are not in this range indicating that the tuning fork design is not robust. To reduce the output variation, either the mean value of the output or the scatter of the most important inputs needs to be decreased. As the first option is meaningless for the frequency of a tuning fork, the second strategy was implemented here. The analysis of the importance of the inputs by their sensitivity measures (Figure 4 (B)) indicates that the scatter of the four most important geometry parameters (grip width, rod length, grip length, rod width) induce ~70 % of the total output variation whereas the E-module induces 26 % of the latter. Consequently, the scatter of these four geometrical inputs was reduced to 0.2 % and the E-module to 0.8 % relative variation of their mean in a second robustness analysis. Finally, only 1 % of the designs were not in the acceptable variation range of ± 7 Hz. Thus, by actively influencing only the most important inputs scatters, a robust design could be obtained.

Author // Stephanie Kunath (Dynardo GmbH)

This tuning fork example can be provided to you as a tutorial with example files.

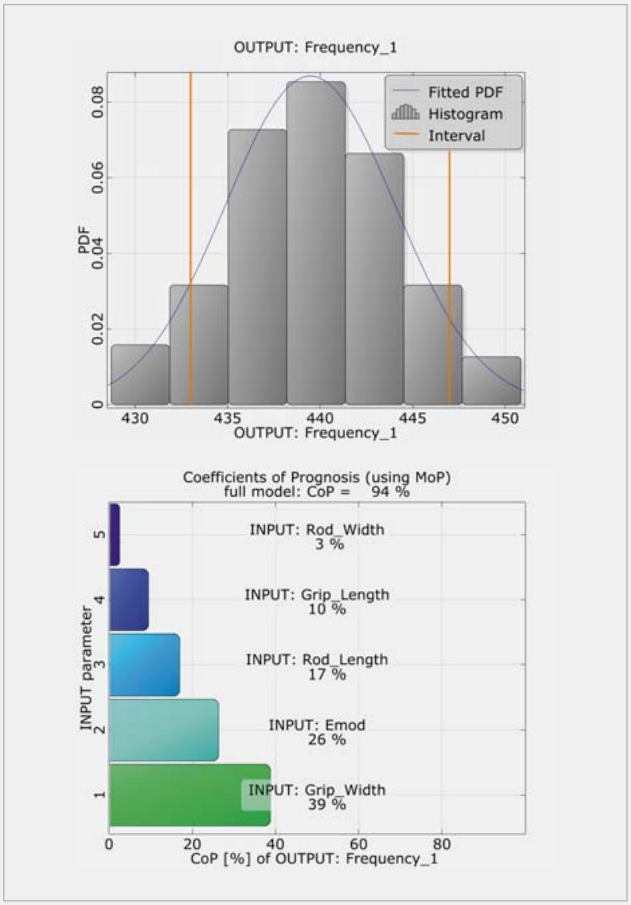

Fig. 4: Results of the robustness evaluation: probability density function of frequency 1 with the interval defining a variation of +/- 7 Hz (top) / CoP values as importance measure for all input parameters that influence frequency 1 (bottom).

CASE STUDY // TURBO MACHINERY

INCREASED EFFICIENCY BY OPTIMIZING THE LAST STAGE OF A STEAM TURBINE

A large gain in efficiency is expected from the optimization of the last stage and the following diffuser of a low pressure turbine (LP) by minimizing losses due to separations as well as inefficient blade or diffuser designs.

Introduction

The energy supply now and in the future is one of the most important issues of our time. It is foreseeable that in the future the energy consumption continues to rise and the supply of coal and other fossil fuels worldwide will decrease. In order to meet future energy needs, in addition to the development of new renewable energy sources, the existing methods for energy production must be as efficient as possible. Further development and the use of modern technologies in power plants, as well as new computational methods for the optimization of turbo machinery, are options for a more economical use of the existing energy resources. But not only increasing the efficiency is one of the key criteria in today's turbo machinery development, in the case of electricity generation mainly the reduced emission of pollutants and, thus, the preservation of the environment, represents an increasingly significant role.

Time efficient optimization methods, as presented here, and the increasing power of computers, make it possible to increase efficiency, which makes it possible to produce more energy under the same amount of resources and, thus, a reduction of pollution compared to a less efficient production.

This article describes an optimization of the last stage of a low pressure steam turbine followed by a diffuser. Since more than 30% of the power is produced in the last two stages of the turbine, this part provides great potential for improving the efficiency of the cold end of the turbine. The resulting losses may be reduced only to a lesser extent by a heat recovery. Therefore, the optimization of the outflow and the conversion of kinetic energy into potential energy by improving the pressure recovery in the diffuser, can decrease the enthalpy at the outlet of the diffuser and so increase the enthalpy difference and thus also significantly improve the system efficiency.

A decisive factor for optimizing this components is the joint consideration of both the last stage and the diffuser. In most cases, the respective components are designed and optimized separately and therefore the full potential for optimization is left aside. Therefore, it will be presented in this article, first a sequential optimization of the last stage followed by a optimization of the diffuser. In comparison, a coupled optimization of both components will be made to show the differences between these two methods. As a

basis for this work, their is a self-made design of a last stage and the diffuser based on information of the industry and literature. In the simulation, next to the flow simulation, a mechanical and dynamical analysis of the stresses and natural frequencies is performed. The calculations are conducted using ANSYS Workbench software. In the first step of optimization, using the optimization software optiSLang, the blades are optimized for fixed diffuser parameters. In the second step, the optimized blades are also fixed and the diffuser is optimized. In the final step, a coupled optimization of diffuser and blades is carried out, starting from the initial design. In the coupled optimization a large number of parameters for both components (51 overall) is involved to also represent the opportunities to solve any large optimization problems efficiently. By the individual optimizations, the sensitive parameters and correlations for the respective outputs and components are also noted.

In the field of optimization of the coupled last turbine stage and the subsequent diffuser, there are already some publications. In most cases, however, the calculations are carried out using 2D codes in order to avoid the high computational cost of 3D simulation. With the constant improvement of computer power and more efficient numerical method, it is worthwhile to work on this topic in the 3D area more and more. Overall, all these publications show a clear improvement over the outcome designs that are previously developed sequential.

Application to aerodynamic optimization

In comparative studies on the application of the deterministic optimization for aerodynamic optimization *Müller-Töws (2000); Sasaki et al. (2001); Shahpar (2000)* usually stochastic programming algorithms or response surface methods *Pierret and Van den Braembussche (1999)* are used in turbo machinery design, for example in the development of engine components, such as at *Vaidyanathan et al. (2000)*. In *Shyy et al. (2001)* a comprehensive overview is represented.

An example of an applied aerodynamic deterministic optimization using a genetic algorithm is published in *Trigg et al. (1997)* and the optimized design of transonic profiles also using genetic algorithms is given in *Oyama (2000)*. Another very comprehensive study of the use of the combination of genetic algorithms and neural networks for two dimensional aerodynamic optimization of profiles is presented in *Dennis et al. (1999)*, who combined a genetic algorithm with an gradient based optimization method.

Application to coupled optimization of the last stage and successive diffuser

One of the first works in this area was published in *Willinger (1997)* in 1997. The aim of this work was not to optimize the coupled components, but in general, to determine the interaction of both components. In particular, the radial gap between rotor and casing was varied, while they observed improvements in the pressure recovery in the diffuser. With increasing the radial gap, the pressure recovery was improved, but with greater flow losses. These losses could not be outweighed by the greater pressure recovery. By increasing the marginal gap, the gap current experiences more energy which allows for certain construction of the diffuser to avoid separations. In particular this has the advantage that shorter lengths of the diffuser are possible, as well as greater diffuser opening ratio. Similarly, in this work, the proposal will be given a numerical optimization to determine further interaction phenomena and to integrate them into the optimization. Also *Jung (2000)* initially dealt only with the phenomena that occur in a coupled calculation and developed in his work an efficient numerical method for the calculation of the coupled model. An optimization is presented for example in *Kreitmeier and Greim (2003)* using a low pressure turbine stage and a subsequent axial radial diffuser. Here, the diffuser has been optimized under fixed blade geometry. The optimization was carried out using a numerical method and in a second sample using an experimental optimization. Both methods achieved significantly better performance than comparable standard designs. The best result came from a 3 channel diffuser. Further work on this area was performed by *Fan et al. (2007)* in a coupled optimization. It turned out that the inhomogeneous flow of the output stage are one of the main reasons for separations in the diffuser. By optimizing the coupled system, also a much better overall performance was achieved. In *Stüer and Musch (2008)* a coupled optimization is also carried out with the focus on the influences of the tip jet, the influence of the flow on the diffuser is investigated with the background of the CO_2 reduction. One result of this work was the development of an efficient method for determining the release tilt of the diffuser, which makes, coupled with an optimizer, very quickly a streamlined design of a diffuser possible. One of the probably most recent work in this area represents *Musch et al. (2013)*. In this work, both last stage and diffuser, were optimized using a "covariance matrix adaptation". To reduce the high computational complexity of this optimization a 2D through-flow code called "'SLEQ'" by *Denton (1978)* was first used and then were the results validated in a further step using a 3D simulation. Result of this work was that a significantly greater potential exists for a coupled optimization. The physical explanation for this greater potential lays in the fact, that the pressure distribution in the outlet of the last stage is the inlet pressure distribution of the diffuser. Therefore, it was also recognized that diffusers, which are based on standard correlations, always lead to a not fully utilized overall performance. A similar work can be found in *Burton et al. (2012)*.

Numerical Model and Simulation

For this work a geometry of the last stage and the diffuser was made based on information from industry. The first developed model was improved by hands, until it was nearly comprehensive with machines in the industry, so that the optimization is also in an area of practical importance.

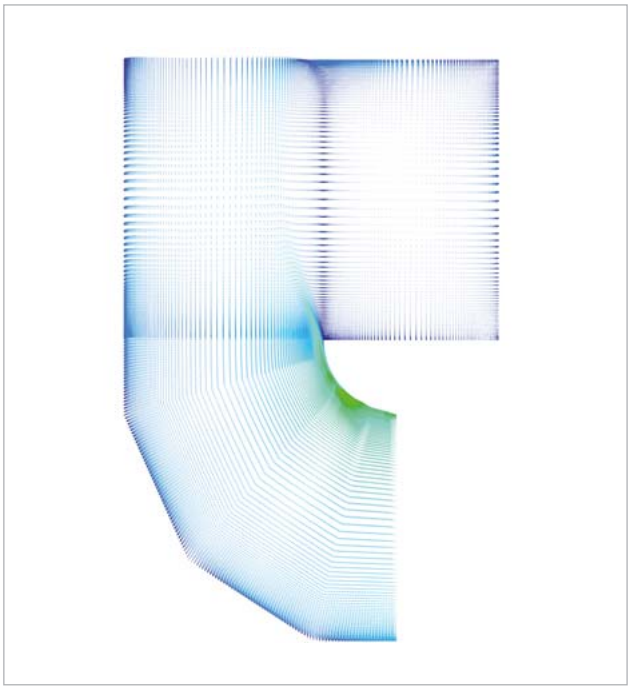

Fig. 1: Velocity profile of the initial diffuser

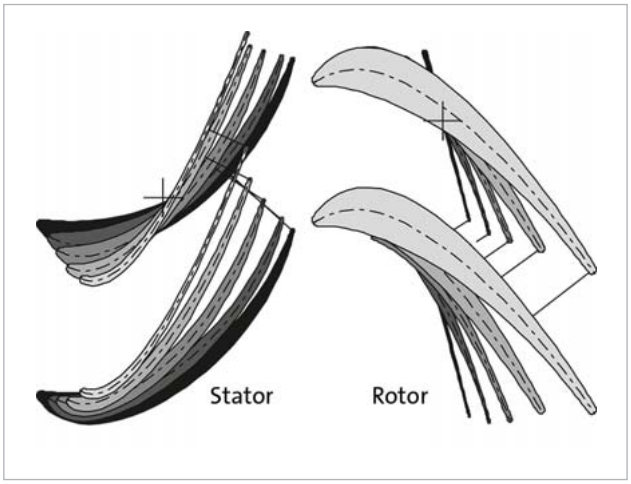

Fig. 2: Geometry of the profiles for stator and rotor

Therefore the guidelines from *Wilson and Korakianitis (1998)* were used to get a first acceptable model of the last stage. In fact that in *Wilson and Korakianitis (1998)* 16 parameters are used to describe a blade section and in ansys bladegen, which was used for the geometry creation in the simulation, only 8 parameters are possible to define, there was a transfer needed to rebuild the model in ansys bladegen with these 8 parameters shown in Fig. 2. As it is shown, the rotor hub profile is more like a reaction type blade then a typical low degree reaction type blade, which is more often used for low pressure steam turbine blades. The advantage of this is that the friction losses in the boundary layers are relatively low at this section. But this was not the main reason for this type of geometry, in the development of the blades, it comes to separations in this area if the reaction type was lower as it is shown in 2. The result is that there is high gradient for the velocity and pressure from hub to shroud, which can be seen in 11 and 13. In real applications it would be a more uniform distribution.

The same process has been done for the diffuser, which was also build up on information of the industry. There is a simplification made for the diffuser, so that it is axis symmetric. Real used diffusers are not axis symmetric because they have a different geometry in the direction of the condenser. That means for the flow simulation that also the calculated flow is axis symmetric in the diffuser, normally it would be a more complex 3-dimensional flow field. But in this case this simplification also reduces the needed calculation time. In Fig. 1 is shown the 2-dimensional velocity profile of the diffuser of the initial design.

Based on a fully parametric geometry model the software ANSYS Turbogrid and ANSYS Meshing is used to realized an automatic mesh generation with in mean 1.5 mio. hexahedron elements for the last stage used and 180k elements for the diffuser. The CFD simulation is realized by the ANSYS CFX solver in combination with mechanical and dynamic analysis for further restrictions in the optimization with 57k tetrahedra elements in the mean.

The boundary conditions for the CFD simulations, are also based on requirements of the industry. It is performed a steady state analysis with a k- turbulence model and a “total energy” heat transfer model. The used fluid is steam without wetness effects. For the inlet of the stage a pressure profile combined with a velocity profile from a real existing low pressure turbine was defined. Also the static temperature of 320 K was set. The setting for the turbulences

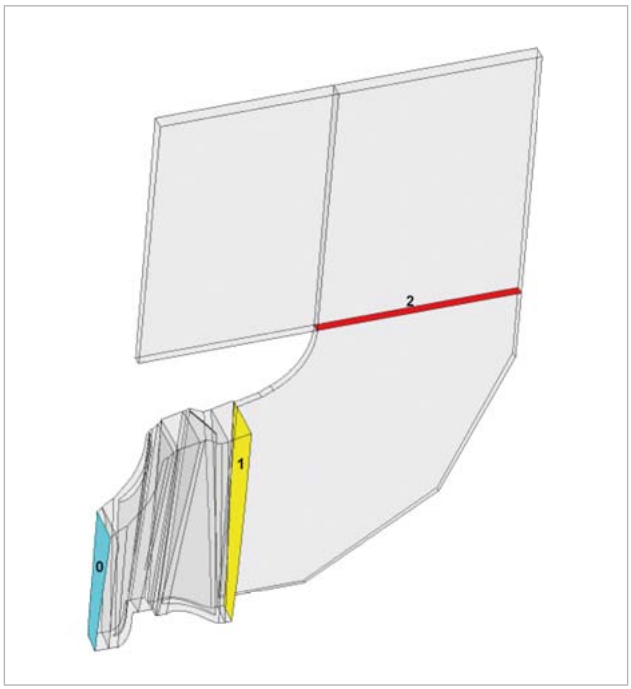

Fig. 3: Used section 0, 1, 2 for the calculation of the output variables

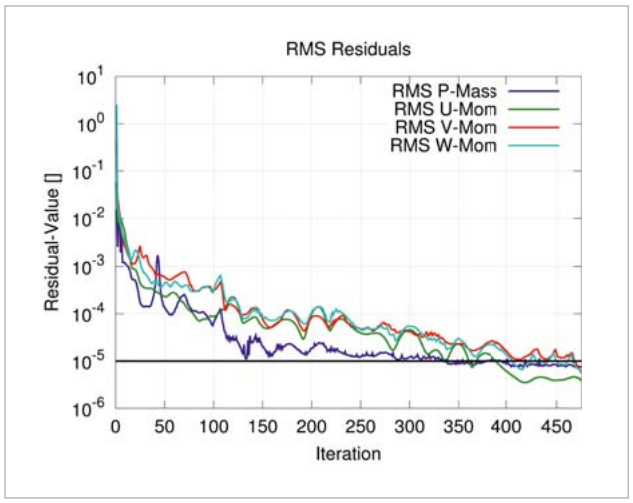

Fig. 4: RMS residuals of the CFD simulation.

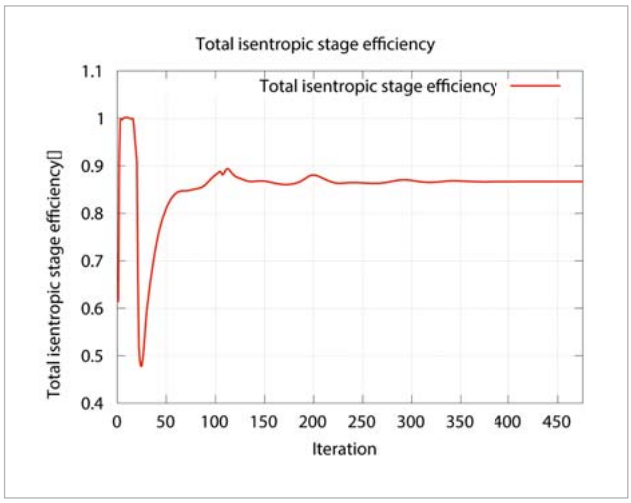

Fig. 5: Convergence of the total isentropic stage efficiency

in the inlet was medium intensity (5%). In the outlet the condenser pressure was 5.500 Pa. For the interface between stator/rotor and rotor/diffuser there was used the mixing model "'stage"'. The stage model uses the averaged circumferential flow informations, so that there is a 2-dimensional flow field information transferred to the diffuser. So there is a 3D model for one pitch length for the stage with periodic boundary conditions and a 2D model for the diffuser with rotational symmetry. The rotor tip jet is also considered due to the fact, that it has a high influence on the diffuser especially on possible separation effects. The used sections to calculate the output values are shown in Fig. 3, according to the indices 0, 1, 2 in the formulas of the outputs.

For the mechanical and dynamical boundary conditions the rotation speed is equal to 50 s−1. The influences of the pressure and temperature of the CFD analysis were not considered, because they are marginal next to the influence of the centrifugal force. The material used for the blades was X5CrNiCuNb16-4 (Material specs from Edelstahlwerke (2008)). In Fig. 4 shows the convergence of the RMS residuals. After nearly 500 Iterations the residuals confirm the stop criteria of 1e-5, according to Ansys (2012), this represents a sufficiently good convergence for such applications. For the optimization different output values are used as optimization objective or as restrictions, which are shown in the tabs. 2, 4, 5. Next to the RMS residuals there were also proved that the output parameters reach a convergent result, for example shown for the total isentropic stage efficiency in Fig. 5.

Optimization

Optimization process

Optimization is defined as a procedure to achieve the best outcome of a given objective function (sometimes also called cost function) while satisfying certain restrictions.

The deterministic optimization problem:

$$\begin{aligned} f(d_1, d_2, \dots d_{\mathrm{n_d}}) &\rightarrow \min \\ e_{\mathrm{l}}(d_1, d_2, \dots d_{\mathrm{n_d}}) &= 0;\ l = 1, n_{\mathrm{e}} \\ u_{\mathrm{m}}(d_1, d_2, \dots d_{\mathrm{n_d}}, \boldsymbol{\gamma}) &\geq 0;\ m = 1, n_{\mathrm{u}} \\ d_{\mathrm{l_i}} \leq d_{\mathrm{i}} &\leq d_{\mathrm{u_i}} \\ d_{\mathrm{i}} \in [d_{\mathrm{l_i}}, d_{\mathrm{u_i}}] &\subset \mathbb{R}^{n_d} \end{aligned}$$

is defined by the objective function $f : \mathbb{R}^{n_d} \rightarrow \mathbb{R}$ subject to the restrictions, defined as equality and inequality constraints e_{l} and u_{m}. The variables $d_1, d_2, \dots d_{\mathrm{n_d}}$ are the optimization or design variables and the vector of the partial safety factors $\boldsymbol{\gamma}$ ensures the system or design safety within the constraint equations u_{m}, for example defining a safety distance $u(\mathbf{d}, \gamma) = y_{\mathrm{g}}/\gamma - y_{\mathrm{d}} \geq 0$ between a defined limit state value y_{g} and the nominal design value y_{d} of a physical response parameter $y = f(\mathbf{d})$. In structural safety assessment, a typical constraint for the stress is given as

$$u(\mathbf{d}, \gamma) = \sigma_{\mathrm{y,k}}/\gamma - \sigma_{\mathrm{d}} \geq 0$$

ensuring the global safety distance

$$\Delta_\gamma = \sigma_{\mathrm{y,k}} \left(1 - \frac{1}{\gamma}\right)$$

between the defined quantile value $\sigma_{\mathrm{y,k}}$ of the yield stress and the nominal design stress σ_{d} with the global safety factor γ. Whereby, in the real approach with given uncertainties, σ_{d} corresponds to the mean of Mises equivalent stress $\bar{\sigma}_{\mathrm{e}}$ at the current design point.

Global variance-based sensitivity analysis

A global variance-based sensitivity analysis, as introduced in *Saltelli et al. (2008)*, can be used for ranking variables $x_1, x_2, \dots, x_{n_r}$ with respect to their importance for a specified model response parameter

$$y = f(x_1, x_2, \ldots, x_n)$$

depending on a specific surrogate model $\tilde{y}$. In order to quantify and optimize the prognosis quality of these meta-models, in *Most and Will (2012)* the so called Coefficient of Prognosis

$$\mathrm{CoP} = 1 - \frac{\mathrm{SSEP}}{\mathrm{SST}} \quad 0 \leq \mathrm{CoP} \leq 1$$

of the meta-model is introduced. In contrast to the commonly used generalized coefficient of determination R^2 which is based on a polynomial regression model, in this equation, variations of different surrogate models $\tilde{y}$ are analysed to maximize the coefficient of prognosis themselves. In the equation above, SSEP is the sum of squared prediction errors. These errors are estimated based on cross validation and gives some indication of the predictive capability of the surrogate model. SST is the sum squares and the equivalent to the total variation. This procedure results in the so called Metamodel of Optimal Prognosis, used as surrogate model $\tilde{y}$ with the corresponding input variable subspace which gives the best approximation quality for different numbers of samples, based on a multi-subset cross validation obtained by latin hypercube sampling *Huntington and Lyrintzis (1998)*. The single variable coefficients of prognosis are calculated as follows

$$\mathrm{CoP_i} = \mathrm{CoP} \cdot \tilde{S}_{\mathrm{T_i}}$$

with the total sensitivity indices

$$\tilde{S}_{\mathrm{T_i}} = 1 - \frac{V_{x_{\sim i}}(E_{\mathrm{x_i}}(\tilde{y} \mid x_{\sim \mathrm{i}}))}{V(\tilde{y})}$$

which have been introduced in *Homma and Saltelli (1996)*, where $E_{\mathrm{x_i}}(V(\tilde{y}|x_{\sim \mathrm{i}}))$ is the remaining variance of $\tilde{y}$ that would be left, on average, if the parameter of x_{i} is removed from the model. In the equation shown above, $x_{\sim \mathrm{i}}$ indicates the remaining set of input variables. In order to estimate the first order and total sensitivity indices, a matrix combination approach is very common *Most (2012)*.

Optimization process in this work

The process of the optimization is shown in the Fig. 6. First before each component gets optimized, a sensitivity analysis is performed to determine the sensitive parameters for each output parameter and their correlations. Therefore a Latin hypercube sampling (LHS) is made with N = 2 · (Inputparameters + Outputparameters) designs calculated. That means there were 107 designs for the rotor optimization, 83 designs for the diffuser optimization and 130 for the coupled optimization. The Latin hypercube sampling is a advanced method of the monte carlo simulation, which made equal distributed designs in their parameter space. Following that,

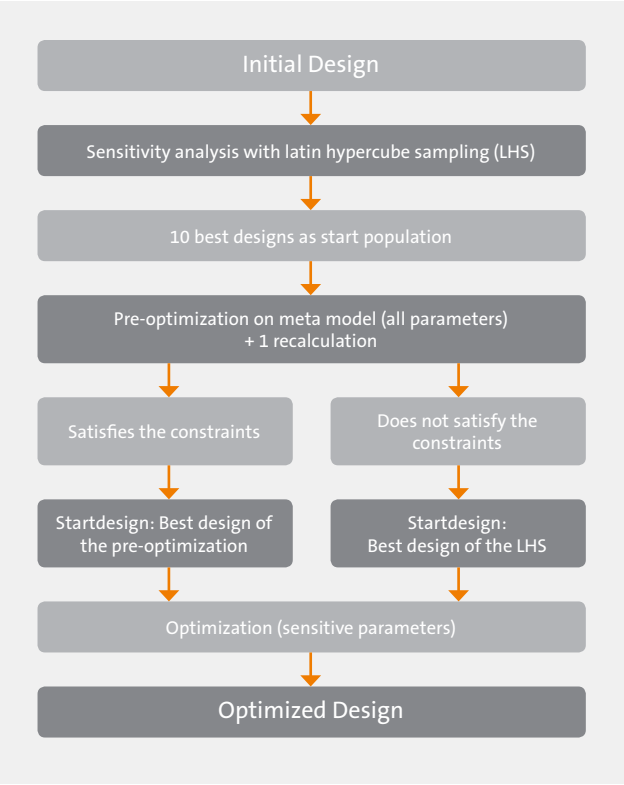

Fig. 6: Overview of the optimization process

a pre-optimization is based on the information of the Latin hypercube sampling creating a meta-model. That means the meta model will be created through the information of the calculated design in the Latin hypercube sampling. The 10 best designs of the Latin hypercube sampling are selected as the starting population for an evolutionary optimization algorithm with all parameters available for each component. These calculations are not carried out in ANSYS, but on the basis of the meta-model. Therewith, it is possible to calculate in a few minutes many designs, to obtain a better design without the use of time expensive calculations. Subsequently, the best design of the pre-optimization will be selected and recalculated in ANSYS. If this design fulfils the constraints it will be used as a start design for a adaptive response surface method (ARSM) optimization, but this time each design is calculated in ANSYS and only sensitive parameters for the respective objective functions and constraints are active. This recalculation depends on how good the meta model is. So it might be possible, that some output have a deviation in the recalculation. If then the constraints are violated this design can not be chosen as a start design for the following optimization. In this case the best design of the LHS will be taken for the further optimization. Possible reasons for such deviations are e.g. strong non-linear physical behaviours or problems with meshing or wrong simulation settings. The prognosis ability is made through a so called coefficient of prognosis (CoP), which gives a percentage value of how good is the output value describable through the input variables. If these values are rather low (≤ 50) it can be expected, that the recalculation will have strong deviations.

Type	Description	Formula	Unit
Constraint	$(h_{\text{in\_h}} - h_{\text{in\_l}}) \cdot 1,2 \geq l_{\max}$	$u_1(\mathbf{d}) = (h_{\text{in\_h}} - h_{\text{in\_l}}) \cdot 1,2 - l_{\max} \geq 0$	[m]
Constraint	$\frac{(2 \cdot \pi \cdot h_{\text{out}} \cdot l_{\text{out}})}{((h^2_{\text{in\_h}} - h^2_{\text{in\_l}}) \cdot \pi)} \geq 2$	$u_2(\mathbf{d}) = \frac{(2 \cdot \pi \cdot h_{\text{out}} \cdot l_{\text{out}})}{((h^2_{\text{in\_h}} - h^2_{\text{in\_l}}) \cdot \pi)} - 2 \geq 0$	$[m^2]$
Constraint	$t_{\text{LE\_**}} \geq t_{\text{TE\_**}}$	$u_3(\mathbf{d}) = t_{\text{LE\_**}} - t_{\text{TE\_**}} \geq 0$	[m]
Constraint	$\lvert f_{\text{ith}} \rvert$ needs to be at least $5s^{-1}$ away of $f_{0\text{th}}$	$u_4(\mathbf{d}) = \lvert f_{\text{ith}} - f_{0\text{th}} \rvert - 5 \geq 0$	$[s^{-1}]$
Constraint	$\gamma_{\text{r}} \geq 1.5$	$u_5(\mathbf{d}) = \gamma_{\text{r}} - 1.5 \geq 0$	
Constraint	$\gamma_{\text{eqv}} \geq 1.5$	$u_6(\mathbf{d}) = \gamma_{\text{eqv}} - 1.5 \geq 0$	
Objective	Total isentropic stage efficiency η_{st}	$f_1(\mathbf{d}) = \frac{\frac{T_{\text{ex,1}}}{T_{\text{in,0}}} - 1}{(\frac{p_{\text{ex,1}}}{p_{\text{in,0}}})^{\frac{\kappa-1}{\kappa}} - 1}$	
Objective	Specific performance $P/\dot{m}_{\text{in}}$	$f_3(\mathbf{d}) = \frac{2 \cdot \pi \cdot M \cdot f_{\text{oth}}}{\dot{m}_{\text{in}}}$	$[Jkg^{-1}]$

Tab. 1: Constraints $u_m(\mathbf{d})$ and objective $f(\mathbf{d})$

Symbol	O_{init}	O_{pre}	O_{fin}	Unit
AR	1,44	1,44	1,44	
$P/\dot{m}_{\text{in}}$	1,415e5	1,431e5	1,395e5	$[Jkg^{-1}]$
c_{pr}	0,579	0,561	0,435	
$\dot{m}_{\text{in}}$	76,636	77,075	77,126	$[kgs^{-1}]$
η_{st}	0,867	0,879	0,886	
σ_{r}	7,948e8	8,811e8	8,661e8	N/m^2
σ_{eqv}	8,287e8	8,087e8	7,931e8	N/m^2
γ_{eqv}	1,553	1,591	1,622	
γ_{r}	1,577	1,434	1,469	
f_1	82,97	83,75	85,09	$[s^{-1}]$
f_2	190,55	181,25	177,56	$[s^{-1}]$
f_3	174,13	231,82	232,54	$[s^{-1}]$

Tab. 2: Overview for each optimization step after the final optimization of the rotor blades

In the following, this procedure will be repeated, for the rotor, diffuser and the coupled system. The constraints for the optimization regarding the geometry of the blade and diffuser are resulted mainly from the industry through guidelines. Additional constraints were safety factors for the stresses and a minimal distance of the eigenfrequencies to the machine frequency. For the objective the were two Output used. First for the rotor optimization the total isentropic stage efficiency and second for the diffuser and coupled optimization the specific performance as shown in Tab. 1.

Sequential optimization work flow

As the first step the optimization of the rotor blades is realized. Which means that the parameters of the diffuser are deactivated for this process. In Fig. 7 the parametrization for the blade is shown. According to five profile sections with eight parameters, in total 40 parameters for the blade optimization are given. The leading and trailing edge are described through two radii, which result out of the other parameters. The target of this first optimization process is to maximize the isentropic stage efficiency η_{st}.

As a result of the sensitivity analysis, the coefficients of prognosis can be used to measure the importance of the input variables. One example is shown in Fig. 8 for the isentropic stage efficiency. The largest variance of the efficiency is described by the profile at 75% of the blade span. Fig. 9 shows the meta-model of the total isentropic stage efficiency in the subspace of the most important parameters.

The results after the adaptive response surface method optimization and the preoptimization in comparison to the initial design are shown in Tab. 2 with an increasing of the efficiency of nearly 2% in addition to compliance with the constraints.

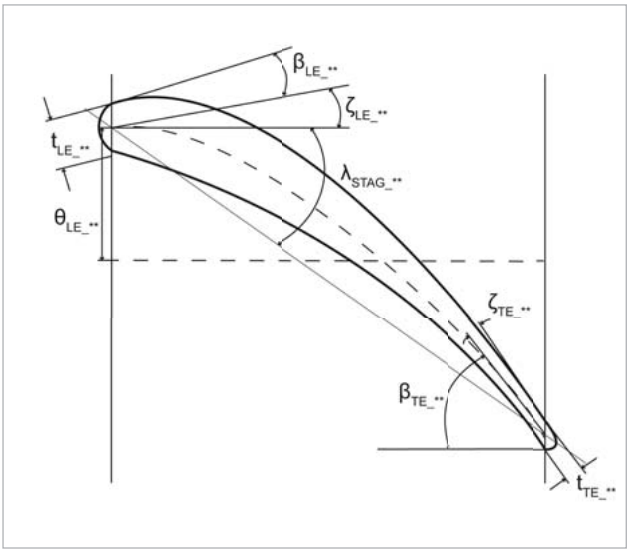

Fig. 7: Overview of the rotor parametrization

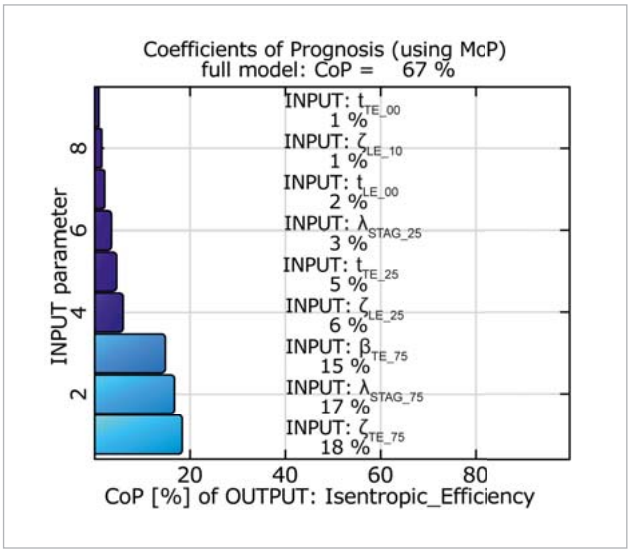

Fig. 8: Most important parameters for the total isentropic stage efficiency

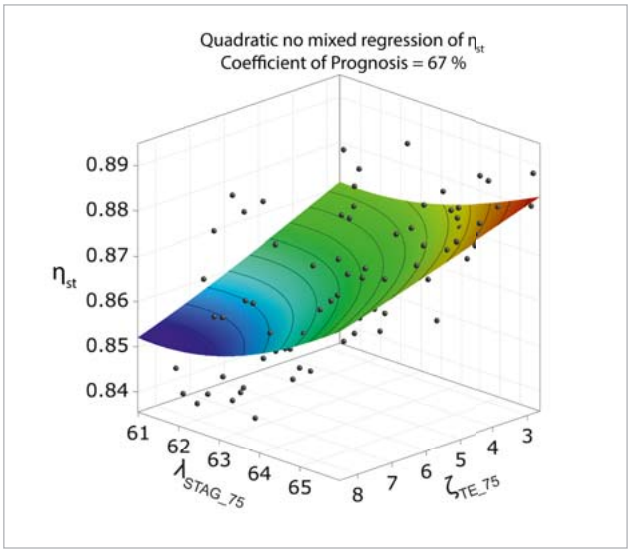

Fig. 9: Total isentropic efficiency and the most important parameters

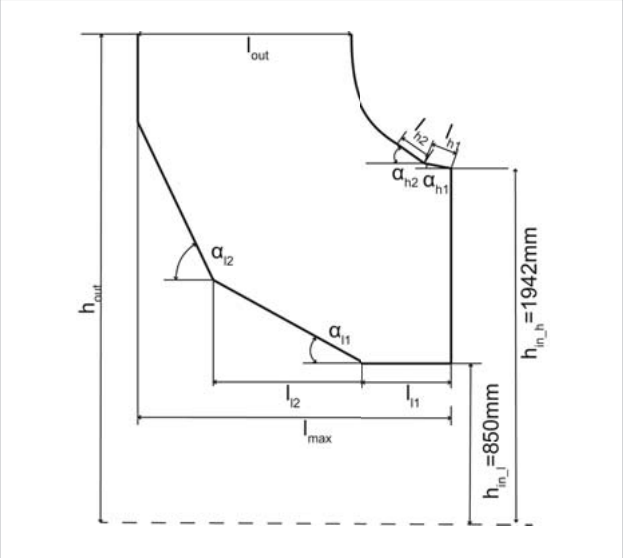

Fig. 10: Diffuser parametrization

Symbol	Metamodel	Recalulation	Difference	Unit
$P/\dot{m}_{\mathrm{in}}$	1,415e5	1,431e5	1,395e5	$[Jkg^{-1}]$
c_{pr}	0,579	0,561	0,435	

Tab. 3: Differences between meta-model and recalculation of the diffuser preoptimization

After the blade optimization, the diffuser optimization is performed. Fig. 10 shows the parametrization. Therefore, 11 parameters are used for the diffuser optimization. The objective for this optimization was the specific performance, because now the optimizer should reach the best performance out of both components with changing the diffuser parameters. It has also been possible to take the pressure recovery as the objective because performance and pressure recovery are correlated. As already described, a preoptimization was carried out based on a meta-model, for each optimization. Table 3 shows as an example of the very small differences between the approximated calculation and recalculation demonstrated on the diffuser pre-optimization. So that this method is a useful tool to perform fast calculations under some circumstances with great improvements as presented here.

Symbol	O_{init}	O_{pre}	O_{fin}	Unit
AR	1,44	1.384	1,417	
$P/\dot{m}_{\mathrm{in}}$	1,395e5	1,416e5	1,418e5	$[Jkg^{-1}]$
c_{pr}	0,435	0,478	0,508	
$\dot{m}_{\mathrm{in}}$	77,126	77,075	77,174	$[kgs^{-1}]$
η_{st}	0,886	0,884	0,883	

Tab. 4: Overview for each optimization step after the final optimization of the diffuser

The final results of the diffuser optimization and thus the sequential optimization are shown in Tab. 4. This time the initial designs stand for the optimized design of the rotor optimization. The resulting increasing of the specific performance is very low, because it is not possible for the optimizer to get a better design out of diffuser optimization. The diffuser is limited to the fixed flow field of the last stage. This means, it is just possible to get a more improved specific performance with changing the flow field in the diffuser. This is reached in this case through increasing the pressure recovery. But as shown there is not a lot of further potential available.

Symbol	O_{init}	O_{pre}	O_{fin}	Unit
AR	1,44	1,44	1,46	
$P/\dot{m}_{\mathrm{in}}$	1,415e5	1,431e5	1,445e5	$[Jkg^{-1}]$
c_{pr}	0,579	0,561	0,571	
$\dot{m}_{\mathrm{in}}$	76,63	77,07	77,29	$[kgs^{-1}]$
η_{st}	0,867	0,879	0,885	
σ_{r}	7,948e8	8,811e8	8,352e8	N/m^2
σ_{eqv}	8,287e8	8,087e8	8,403e8	N/m^2
γ_{eqv}	1,553	1,591	1,531	
γ_{r}	1,577	1,434	1,501	
f_1	82,97	83,75	84,26	$[s^{-1}]$
f_2	190,55	181,25	173,46	$[s^{-1}]$
f_3	174,13	231,82	216,43	$[s^{-1}]$

Tab. 5: Overview for each optimization step after the final optimization of the coupled optimization

Coupled optimization work flow

The last step is the coupled optimization of the rotor and diffuser. Now, the specific power is used as the optimization target. The optimization results are presented in Tab. 5. As

shown in this table the specific performance is much better in comparison with the sequential optimization. The optimizer reaches the same level of stage efficiency like the

d_o	O_{rot}	O_{dif}	O_{cp}
$P/\dot{m}_{\mathrm{in}}$	$\lambda_{\mathrm{STAG\_75}}$ $t_{\mathrm{LE\_75}}$ -	l_{out} h_{out} l_{max}	$\lambda_{\mathrm{STAG\_75}}$ l_{out} -
c_{pr}	$\lambda_{\mathrm{STAG\_75}}$ $\lambda_{\mathrm{STAG\_10}}$ $t_{\mathrm{LE\_75}}$	l_{out} h_{Out} -	$\lambda_{\mathrm{STAG\_75}}$ h_{Out} $\lambda_{\mathrm{STAG\_50}}$
η_{st}	$\zeta_{\mathrm{TE\_75}}$ $\lambda_{\mathrm{STAG\_75}}$ $\beta_{\mathrm{TE\_75}}$	h_{out} - l_{out}	$\lambda_{\mathrm{STAG\_75}}$ $\beta_{\mathrm{TE\_75}}$ $\zeta_{\mathrm{TE\_75}}$

Tab. 6: Overview of the sensitive parameters in the individual optimization steps

output parameters and the constraints is also shown. The result is a specific performance advantage for coupled optimization of 1.8 % compared to the sequential optimization. Furthermore, the pressure recovery with +12.4% and the stage efficiency with +0.2% are better than the sequential optimization results. Only the safety factor of the coupled optimization regarding the von Mises stress is worse at -5.94% as in the sequential optimization, but meet the

	$P/\dot{m}_{\mathrm{in}}$	η_{st} (%)	c_{pr}	γ_{eqv}	γ_{r}
O_{seq}	1,418e5	88,3	0,508	1,622	1,469
O_{cp}	1,445e5	88,5	0,571	1,531	1,501
Δ in %	1,8	0,2	12,4	-5,94	2,1

Tab. 7: Differences between the output parameters of sequential and coupled optimization

sequential optimization but with keeping the pressure recovery as it was in the initial design. That means with the possibility of changing all parameters, the optimizer could change them in a way that both components benefit. This clearly shows the advantage of the coupled optimization compared to the sequential optimization.

Interpretation of results

Table 6 shows an overview of the different output variables and their sensitive parameters in descending order of importance, depending on the optimization steps. Many of the sensitive parameters of the rotor optimization can also be found in the coupled optimization again. Similarly, the same for the significant parameters of the diffuser optimization. Which means that irrespective of whether a coupled or sequential optimization is made, the same key parameters are identified. Maybe, non-observance of diffuser parameters in the rotor optimization will result in wasting of optimization potential. In the sequential optimization there were much more parameters, for example for the blade optimization, taken as really needed, because most of them have got a much lower effect on the objective as in comparison with only one additional parameter of the diffuser, as shown in this table. Furthermore, this overview shows a certain dominance of the influence of parameters on the performance of the blade and the pressure recovery, which also depend on the diffuser. For the comparison of each column the main parameters of the diffuser optimization move under the main parameters of the rotor results in the optimization of the coupled optimization.

Thus, a further advantage of the coupled optimization is to determine the parameters with the greatest impact in the overall system to develop or to exhaust the full potential for a better performance. Therefore, in Tab. 7 the comparison of sequential and coupled optimization of the relevant constraints of ≥ 1.5. Clearly visible is the large influence of a better pressure recovery on the specific power, although there is almost the same stage efficiency for both optimization sequentially and coupled. It should also be noted that only a single parameter (lout) was active in the ARSM of the coupled optimization. One parameter from the diffuser may be enough, to change along with the blade parameters in order to achieve a better overall result.

As a further result, as shown in Fig.s 11-12 and 13-14, the total pressure and velocity profiles in the diffuser inlet and outlet of each optimization step is given for comparison. The overall pressure and velocity distribution in the inlet is nearly equal for all three versions of the diffuser. In the outlet, the distribution of the pressure and velocity of the initial design was much more uniform as it was for the coupled and sequential version. Even so the results for the pressure recovery showed that the initial design and the

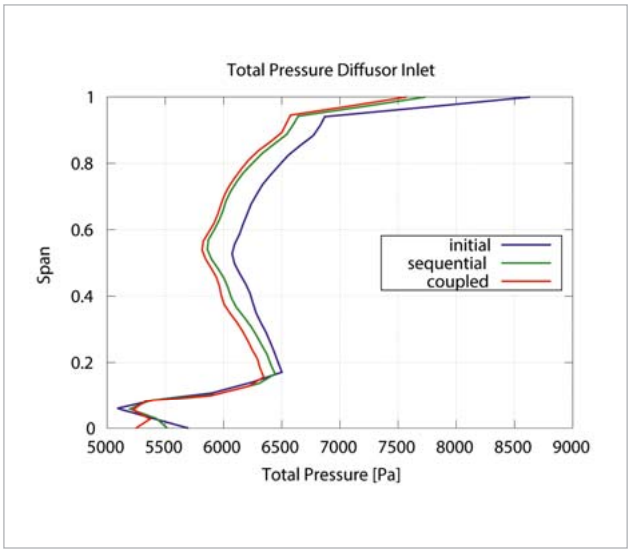

Fig. 11: Pressure profiles in the diffuser inlet of each optimization step

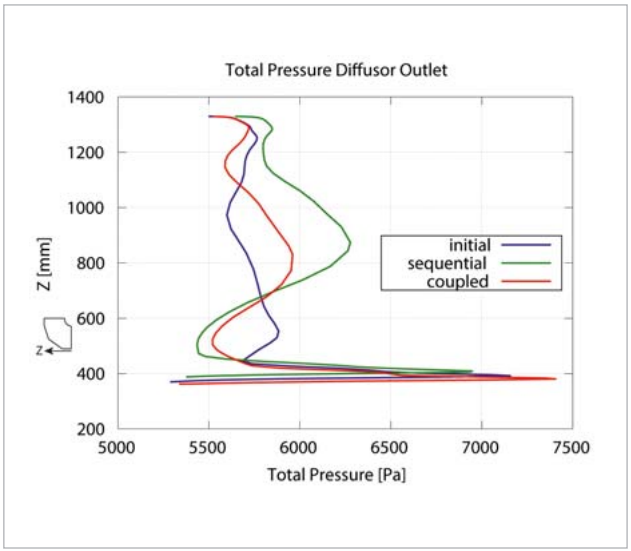

Fig. 12: Pressure profiles in the diffuser outlet of each optimization step

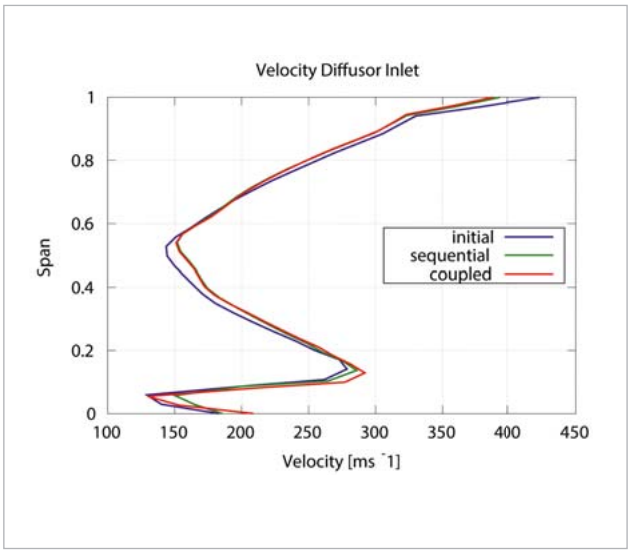

Fig. 13: Velocity profiles in the diffuser inlet of each optimization step

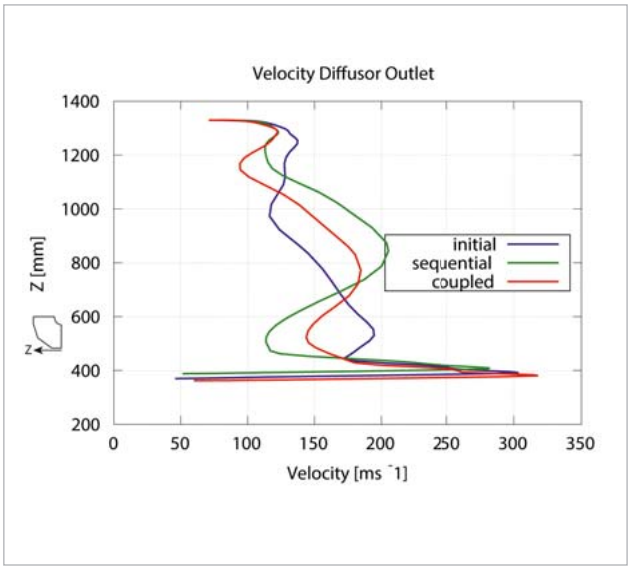

Fig. 14: Velocity profiles in the diffuser outlet of each optimization step

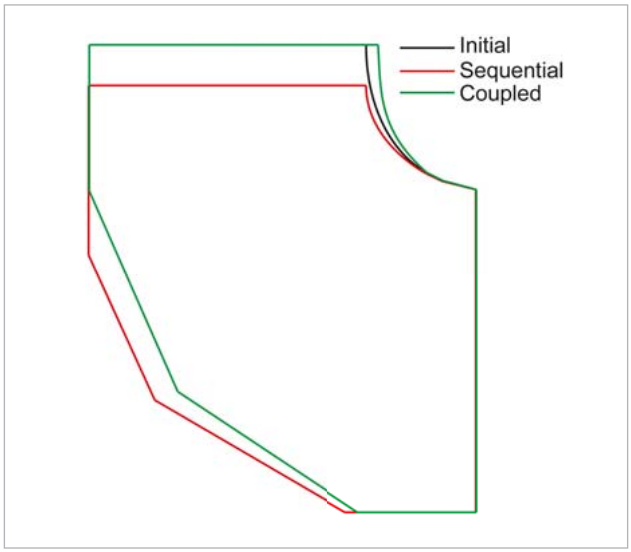

Fig. 15: Superimposed view of the diffuser geometries in the individual optimization steps

coupled optimized design got nearly the same value. The pressure recovery of the sequential optimized design was more worst. This can also be seen in this diagrams. The reduced velocity, which is the result of a diffuser to transfer the kinetic energy into potential energy, is much better for the initial and coupled optimized design. There is a high peak of velocity in the sequential optimized version. So the integral of these curves is much higher for the sequential version as it is for the others, which leads to a overall lower pressure recovery regarding that all three got nearly the same inlet conditions.

Fig. 15 shows the scaled form of the different diffuser geometries. In total 313 designs are calculated with a duration of 33 days and for the coupled optimization and 263 designs with a duration of 28 days for the sequential optimization. As hardware two computers with following specifications are used:

- CPU: 2 x AMD Opteron 6376 with 16 cores, 2.3 GHz
- 64 GB of memory

This computational effort shows whether it makes sense to perform an optimizations using 3D calculations or whether it would be better to use 2D calculations or similar replacement model. The computation efforts for both paths are very long and would probably be too time consuming for use in practice. However, the presented method with a less computationally intensive model or equivalent model and subsequent recalculation in 3D could also be a time efficient way to improve the development of such machines.

Conclusion

The specific performance benefit of the coupled optimization over the sequential optimization is 1.8% in compliance with all constraints. This is mainly explained through a

much better interaction between stage and diffuser. In both optimization methods, a similar high stage efficiency is achieved. However, in the sequential optimization in a way that it prevented the diffuser, to reach a much better overall performance, which is below the overall performance of the coupled optimization. In the coupled variant the same efficiency is achieved, but in such a way that the diffuser could also achieve a very high pressure recovery. During the optimizations the whole parameter space, which is used for both, is equal. Therefore, it can be seen as the final result that the coupled optimization in this work has significant advantages over the sequential. The fact that there is a coupling of the two components since the outlet of the stage and thus the flow field corresponds to the field entry of the diffuser. Both have influence on the performance values of the overall system. Although the flow can be designed that it produces a good stage efficiency for the output stage, but a poor flow field for the diffuser and vice versa.

To give this work a conclusion, there is a recommendation to develop and optimize the last stage and the diffuser in a coupled way to use the full potential of both because:

1. There is a better understanding possible of the relationship of individual performance output parameters and the parameters affecting them across the component boundaries.

2. It can be exhausted additional potential, by simultaneous modification of parameters of both components to a better overall performance.

3. The flow field is adjusted, therewith both components can benefit and not a component is better or worse.

4. It may be more time efficient to develop both components simultaneously.

The authors would like to express their thanks to C. Musch of the Siemens AG for his assistance of collaborative method implementation into the CAE process.

Authors // K. Cremanns / D. Roos, A. Graßmann (Niederrhein University of Applied Sciences)

Source // www.dynardo.de/en/library

Nomenclature

$\dot{m}$	Mass flow of the stage inlet $[kg/s]$
η_{st}	Total isentropic stage efficiency
$P/\dot{m}_{\mathrm{in}}$	Specific performance $[Jkg/s]$
c_{pr}	Pressure recovery
σ	Stress
γ	Safety factor
f	Eigenfrequency $[s^{-1}]$
AR	Diffuser outlet area/inlet area
d	Parameter
O	Optimization
h	height
t	thickness
$\mathrm{l},\ \Theta$	length
P	Pressure
$\alpha, \beta, \lambda, \zeta$	Angle
T	Temperature
CoP	Coefficient of Prognosis
κ	Isentropic exponent
M	Torque

Subscripts

init	Initial
pre	Previous
fin	Final
seq	Sequential
cp	Coupled
rot	Rotor
i	Input
ith	1-3th Eigenfrequency
o	Output
eqv	von Mises equivalent stress
r	Radial stress
in	Inlet
out	Outlet
TE	Trailing edge
LE	Leading edge
STAG	Stagger angle
$\_**$	Span at 0, 25, 50, 75, 100 %
dif	Diffusor
0	Stator inlet
1	Rotor outlet/ Diffuser inlet
2	Diffuser outlet

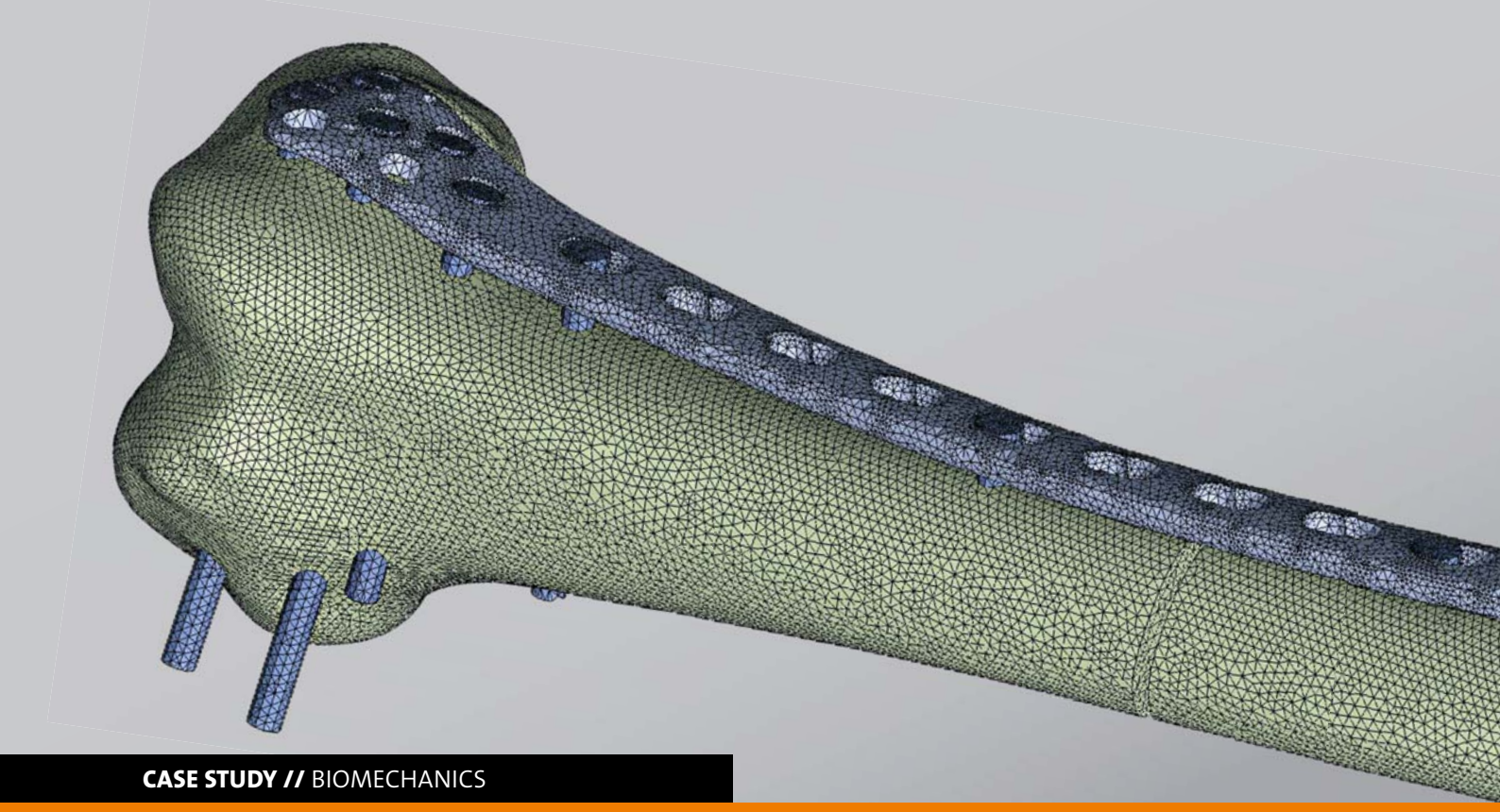

OPTIMIZATION OF FRACTURE TREATMENT

By using optiSLang and ANSYS, the finite element analysis enables surgeons to design and to optimize patient-specific screw arrangements and positions on locking compression plates in diaphyseal fractures of the femur. The analysis and optimization can be conducted within an automated procedure.

Introduction

The incidence of femoral shaft fractures is reported as being 1 fracture per 10,000 people. This rate increases to 3 fractures per 10,000 people for male individuals younger than 25 years and elderly patients, especially women, above the age of 65 years. The causes for the fractures of young males mainly include traffic or sports accidents. The increase in femoral fractures among elderly patients is due to an increase in osteoporosis and often results from low-energy trauma, such as falls from standing height at home. With an increase in life expectancy, the overall number of femoral fractures among elderly patients due to osteoporosis is expected to rise. Regarding these patients, an adequate treatment of femoral fractures which takes the material properties of osteoporotic bone into account, is important for a fast remobilization of the patients.

The focus of this study was the treatment of femoral shaft fractures which are commonly treated with plate osteosynthesis. The plate osteosynthesis involves bringing the ends of a fractured bone together and fastening them with a metal plate and screws. Although there are a variety of different plate types, locking compression plates have been widely applied in recent years. Among patients with osteoporosis, the stable fixation of the plate is a big challenge for the surgeon since the bone often lacks the desired stability. This may lead to a high complication rate due to the loosening of screws or breakage of the plate.

The aim of this study was to support surgeons to decide where to place the screws in order to achieve an optimal fracture healing and to prevent implant failure after a femoral shaft fracture. For this purpose, hundreds of different screw arrangements were evaluated and optimized using optiSLang controlling an automated workflow. The procedure involved:

- the use of computed tomography data for patient-specific modeling of the inhomogeneous material properties of the bone
- the evaluation of biomechanical parameters with finite element analysis
- the optimization of the screw arrangement under given constraints

The constraints for the optimization included the number of screws, the inter-fragmentary movement, the distance between plate and bone as well as the yield material properties of bone, plate and screws.

The automation of this process offered a whole new perspective compared to currently used approaches for investigating the influence of position and number of screws on fracture healing. Without an automated process, only a small number of different layouts could be compared to each other. With the proposed system, however, it was possible to select the best layout of hundreds of designs with reasonable effort.

Background

The process of fracture healing is a complex procedure which depends on a multitude of biological and mechanical factors. The process has been well studied in vitro and in vivo experiments. Based on these experiments, advanced treatment methods for bone fractures utilizing techniques such as plate osteosynthesis have been developed. In addition to in vivo and in vitro experiments, computational methods can also lead to new insights concerning the biomechanics of fracture treatment. For example, finite element analysis has proven to be a powerful tool in the evaluation of deformations and stress distributions under load.

Although "flexible internal fixation" is now regarded as the standard approach for the treatment of long bone fractures, there is still disagreement about the conditions for optimal fracture healing. Many research projects focus on defining parameters for fracture treatment both in vivo and in vitro. The healing of a fracture is influenced by biological (e.g. supply with blood) and biomechanical (e.g. interfragmentary movement) parameters. In addition, implants should not fail under the applied load.

The total number of screws influences the stability of a fracture treatment using a plate as an implant for the bone. If too little screws are used, the construct will be unstable. However, screws damage bone tissue, so, their usage should be kept to a minimum. *Stoffel et al.* suggested that for fractures of the lower extremities, two or three screws on either side of the fracture should be sufficient.

Interfragmentary movement is the relative movement of two pre-defined points on opposite sides of a bone fracture. The formation of solid bone tissue is only possible under stable conditions. Too much movement can cause pseudarthrosis, i.e. non-union, of a fracture. Prohibition of any movement can also lead to delayed healing or non-union of the fracture, since the natural formation of callus is prevented. Therefore, a certain interfragmentary movement is needed to induce fracture healing.

According to these studies, interfragmentary movement between 0.5 mm and 1 mm can be considered optimal. Traditional locking screws face the problem that due to a rigid plate-screw connection, the motion at the fracture gap directly beneath the plate is limited. This side of the bone is referred to as "near cortex". The opposite side of the bone facing away from the plate is referred to as "far cortex". Due to the elasticity of the plate, a bending motion can occur under load. This leads to a higher interfragmentary movement on the far cortex compared to the near cortex. This can cause unequal callus formation on opposite sides of the bone, which results in faster healing on the far cortex compared to the near cortex (Fig. 1).

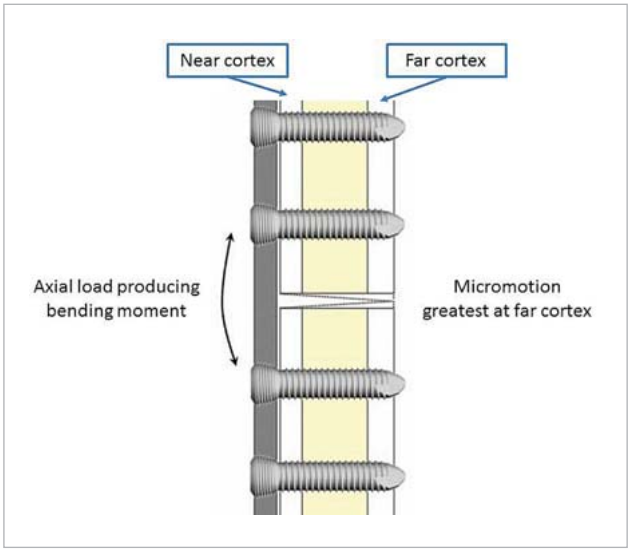

Fig. 1: Fracture movement on the near cortex is limited compared to the far cortex

Objective

The treatment of fractures is a complex process. To ensure an optimal healing process, several biomechanical factors such as the interfragmentary movement have to be considered. The influence of these factors on the healing process has been extensively researched. Currently, it is not possible to guarantee an optimal setting of these parameters during surgery. Surgeons normally base their decision of where to place a screw on experience and general guidelines. However, the structure and shape of the bone of every patient is different. In particular, patients with osteoporotic bones need special attention to prevent bone damage which may lead to implant failure.

This work aims to develop a tool which supports the surgeon in deciding where to place screws during plate osteosynthesis in order to provide optimal healing conditions. For this purpose, an automatic workflow has to be developed which determines the best screw configuration under given constraints. In this workflow, biomechanical parameters, e.g. displacement, stress and strain, on bone and implant have to be evaluated for a multitude of designs. FEA is used

for the assessment of these factors. These parameters are used as parameters for optimizing the screw configuration. The optimization procedure produces one patient specific layouts which satisfies all constraints and offers the best-known healing prospects for the fracture.

To enable use in a clinical setting, the need for user input should be kept to a minimum so that non-specialists are also able to use this tool. In addition, to minimize costs for hospitals, existing software packages should be used. Automation of the whole workflow and an efficient computation time are especially important to ensure quick delivery of results which is essential in a clinical environment

Materials and Methods

A partly automated workflow (Fig. 2) was developed to select the best screw arrangement and position for plate osteosynthesis. Some tasks had to be executed manually for every patient. These tasks included bone segmentation, repositioning of bone fragments as well as the initial positioning of the plate. The majority of tasks, however, were controlled by optiSLang (DYNARDO GmbH, Weimar, Germany) and automatically performed. These tasks included the mesh generation, the assignment of material properties and boundary conditions, the finite element analysis and the optimization. The model consisted of bone fragments, a locking compression plate and a varying number of screws. These objects were either generated or adapted for use in a FEA.

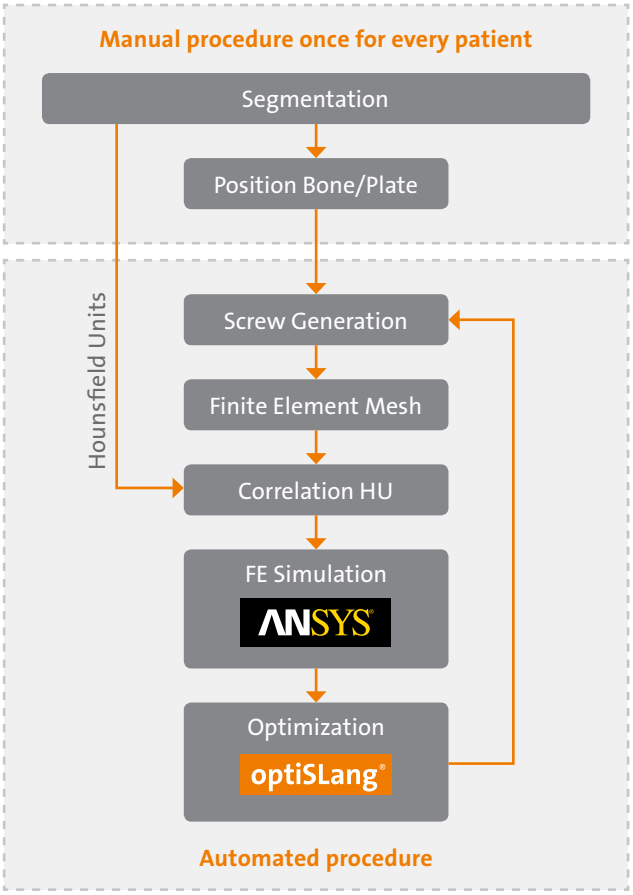

Fig. 2: Procedure for the optimization of fracture treatment

The CT dataset of a 22-year old female was supplied by the Department of Radiology at the Technische Universität München. The software Mimics (Materialise, Leuven, Belgium) was used for the segmentation of the three-dimensional CT data sets. Finally, a three-dimensional geometry of the femur was created. The surface of the bone was smoothed and any small holes, tunnels or peaks on the surface were removed with the software Geomagic (Research Triangle Park, North Carolina, USA). In this study, a healthy femur was used as an example and an artificial transverse fracture with a fracture gap of 3 mm was created using the software Blender Version 2.67 (Blender Foundation, Amsterdam, The Netherlands) (Fig. 3).

Fig. 3: A transverse fracture with a fracture gap of 3 mm was artificially added to a segmented femoral bone

In this simulation, a Locking Compression Plate (LCP, article number: 422 258) manufactured by the company Synthes (Zuchwill, Schweiz) was used. This plate was designed for the treatment of distal femoral fractures. The compression plate had seven screw holes on the distal end and 13 screw holes for the fixation along the bone shaft. The plate was designed to match the mean shape of femoral bones of a cohort and allowed secure attachment. The plate was positioned relative to the femur following the recommendations of surgeons. The screws were automatically generated using the software Blender at the beginning of each optimization loop. An input file contained information about each screw as a discrete variable. The file was generated automatically by the software optiSLang. The value “0” represented the state “no screw”, “1” a monocortical screw and “2” a bicortical screw. To demonstrate the functionality of this model, four screw designs were chosen. The layouts differed with respect to the bridging length, which is the distance between fracture gap and the first screw on either side of the fracture. The bridging length is known to have a large influence on the stability of the plate-bone construct. Four different designs were evaluated: In design a, the screws were placed directly next to the fracture. In design b and c, the bridging length were comprised of two or five unoccupied screws holes respectively. Design d had the largest bridging length with ten empty screw holes (Fig. 4).

The finite element mesh was created with the mesh generation software ANSYS ICEM CFD (ANSYS Inc., Canonsburg, USA).

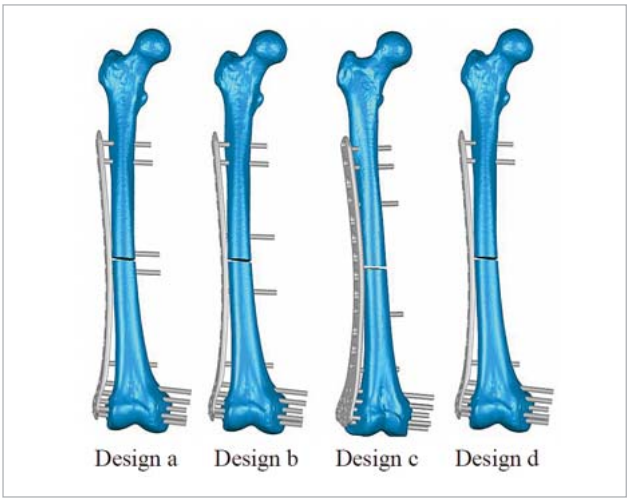

Fig. 4: Four screw layouts with varying bridging length. The bridging length is the distance between fracture gap and the first screw on either side of the fracture

Fig. 5: Meshed bone with plate and screws

The mesh was generated (Fig. 5) automatically reading a script in the programming language tcl (Tool Command Language) using the following procedure:

- Import of stl files
- Create intersection lines and intersection points between objects
- Create material points
- Mesh generation
- Smoothing of mesh surface
- Export of data as input file for ANSYS Classic

Since the arrangement of screws was different for every optimization run, the tcl file was re-generated during every optimization run by a Python program.

The material properties for bone, plate and screws were set in the pre-processor in ANSYS. Plate and screws were considered as homogeneous materials either made of the titanium alloy Ti-6Al-7Nb or stainless steel 316L. Bone was modeled as an inhomogeneous material consisting of 72 different materials depending on the HU value of the element. Cortical bone properties were chosen as the material property for the homogeneous bone to assess the difference between modeling the bone as a homogeneous object compared to an inhomogeneous object. All materials were assumed to be linear elastic and isotropic. Patient-specific bone material properties, such as Young's modulus, were derived from Hounsfield Units contained in CT data. The mechanical properties were mapped onto the mesh using an algorithm programmed in Python.

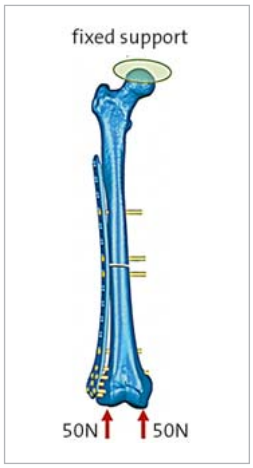

Fig. 6: Physiological loading case - Force application from distal

A number of studies have looked into the physiological loading of femoral bone. However, opinions about the loading vary greatly which might be caused by the complexity of the loading cases. In particular, loading cases shortly after surgery have yet to be researched. Following surgery, patients should put a maximum weight of 10 to 15 kg on the injured leg. At the beginning of the rehabilitation process, patients learn not to put more than a weight of 15 kg on the injured leg. This weight is equal to the ground reaction force (GRF), which is the force exerted by the ground in response to a body being in contact with it. The combined weight force of foot and lower leg added up to approximately 50 N for an average total body weight of 70 kg. The maximum force on the distal end of the femur would be 100 N under the assumption the patient puts a maximum weight force of 150 N on the injured leg (Fig. 6). Half of the force was put on each femur condyle to ensure physiological application of the force. The forces were represented as a vector

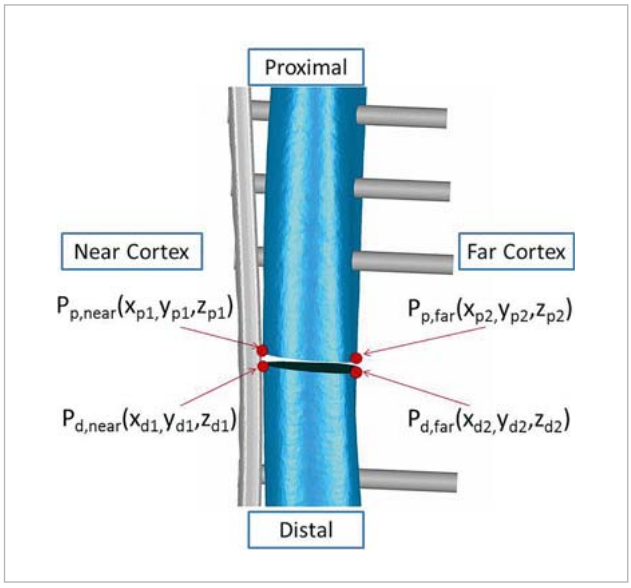

Fig. 7: Determination of interfragmentary movement using the relative displacement of two points on the far cortex and on the near cortex of the bone. (Pp,xxx = Displacement of node on proximal bone fragment, Pd,xxx = Displacement of node on distal bone fragment, d = Relative displacement between two points)

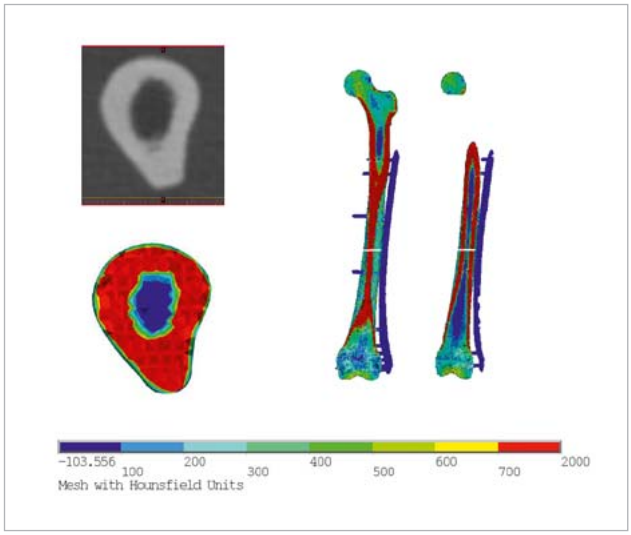

Fig. 8: Assigning HU as temperatures on the finite element model of bone. Left side: CT scan (top) and finite element model with HU distribution (bottom) of femoral shaft bone. Right side: Two parallel longitudinal sections of the finite element model of femoral bone. Cortical bone (red) was mainly located along the bone shaft. The femoral epiphyses primarily consisted of cancellous bone (green). The dark blue array of the bone indicated the bone marrow. No HU were assigned to the plate and screws.

field rather than two single vectors. This led to smoother changes in the internal forces and moments.

Elderly people particularly have problems maintaining a maximum weight of 15 kg on the injured leg. In light of this, the applied force was increased threefold to 300 N to simulate an accidental overload situation.

The relative displacements of two nodes on the near cortex and far cortex were determined for the evaluation of the interfragmentary movement (Fig. 7). These nodes were already defined during the mesh generation stage. HU values were successfully assigned to the elements of the finite element model of the bone (Fig. 8). The bone shaft consisted mainly of cortical bone with HU larger than 700. Cancellous bone was the main material of the femoral epiphyses with HU below 600. Negative HU were assigned to elements of the medullary space. On average, more than 30% of femoral bone was classified as cortical bone.

The elements of the outermost layer were assigned slightly lower HU values than the next inner element layers. This was caused by averaging the HU of bone and the surrounding soft tissue which possessed HU values below that of bone.

Optimization

The sensitivity analysis and optimization were performed using the software optiSLang v4 (Fig 9). New designs were created using an evolutionary algorithm. The objective of the optimization was to minimize the number of screws. The parametric model consisted of 21 design parameters. 20 design parameters were responsible for generating the screws. These parameters could take on one of three discrete states: 0 representing no screw, 1 representing a monocortical screw and 2 representing a bicortical screw. As the subject bone showed no signs of osteoporosis, the same outcomes would be expected no matter if monocortical or bicortical screws were applied. Therefore, only two discrete states were permitted (0 = no screw, 2 = bicortical screw). The remaining design parameter represented the distance between plate and bone. This parameter could take on a continuous value between 0 mm and 5 mm.

The constraints of the optimization were chosen according to findings from the literature. To maintain a stable attachment of the plate to the bone fragments, at least two screws had to be placed in every fragment. The interfragmentary movement was considered an important boundary condition for optimizing the number of screws and their position. Due to the bending load, the interfragmentary movement on the near cortex was generally smaller than on the far cortex. Two constraints

Parameter	Value	Loading
Number of screws per fragment	$n \geq 2$	n.a.
Interfragmentary Movement – near cortex	dnc < 0.7 mm	Normal load
Interfragmentary Movement – far cortex	dfc < 1.7 mm	Normal load
Maximum stress (titanium alloy)	$\sigma < 800$ MPa	Overload (threefold)
Maximum stress (stainless steel)	$\sigma < 690$ MPa	Overload (threefold)
Maximum stress (bone)	$\sigma < 100$ MPa	Overload (threefold)

Tab. 1: Boundary constraints for optimization

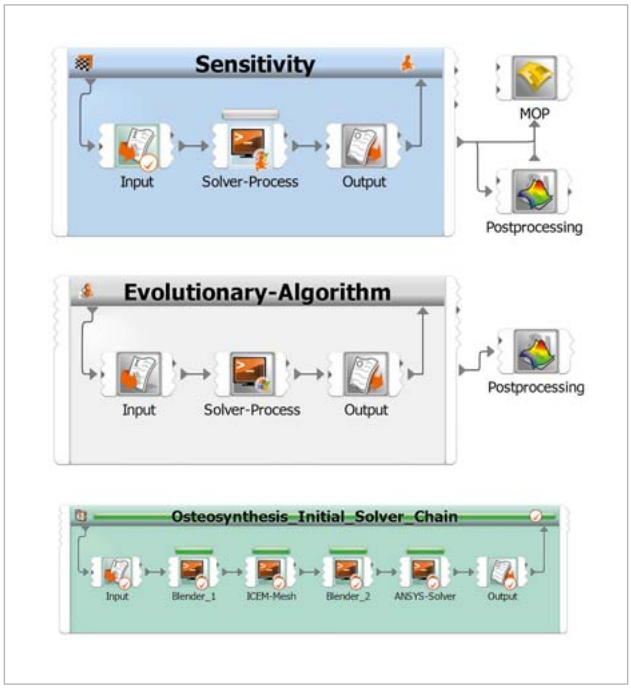

Fig 9: Upper panel: sensitivity work flow with meta modelling; middle panel: optimization work flow; lower panel: solver-chain

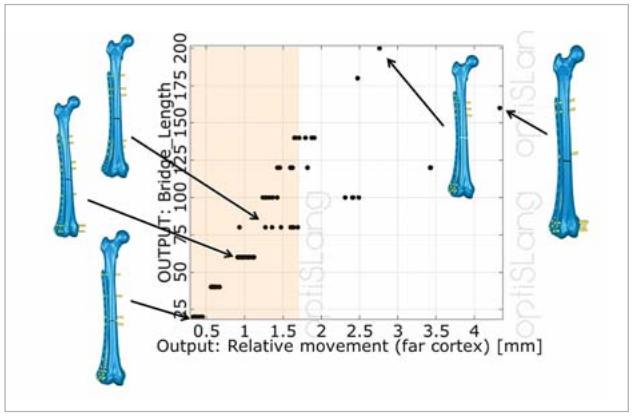

Fig 10: Relationship between bridging length and interfragmentary movement on the far cortex. A linear correlation between the bridging length and the relative movement of the far cortex was observed

gorithm (Fig 11). The design had a medium bridging length of four unoccupied screw holes which equaled a distance of 100 mm. There was a 0.5 mm distance between plate and bone. 180 designs were evaluated in order to select the best design. Designs with up to 16 screws were evaluated during the random sampling period. Primarily designs with four screws were tested towards the end of the optimization.

Discussion

This study developed a general procedure for the optimization of fracture treatment. The aim was to improve the healing process by determining the optimal screw configu-

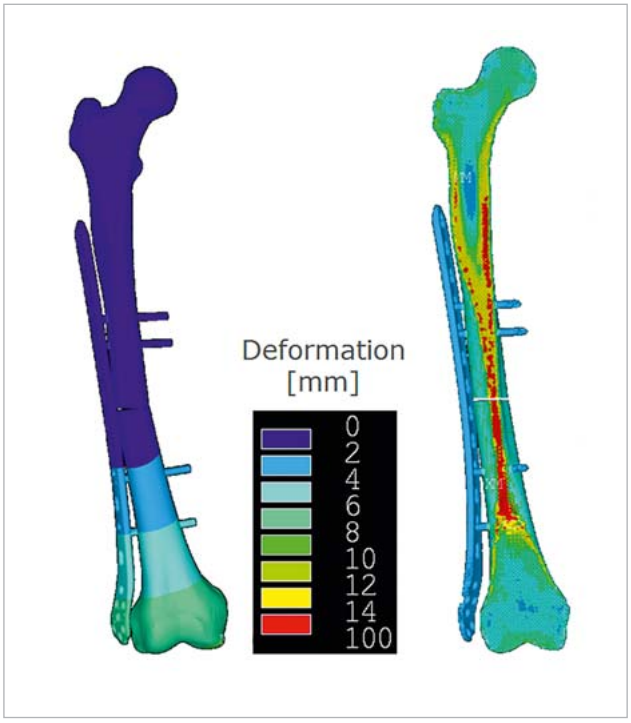

Fig 11: Optimal design after optimization under pre-defined constraints. The optimal design consisted of four screws in total, two screws on the distal segment and two screws on the proximal segment. The bridging length measured 100 mm

were specified to take this behavior into account. To prevent failure of the implant under overload the stress levels in the bone, plate and screws had to remain below the yield stress for the corresponding material. Overload was defined as three times the recommended load. An overview of the parameters and their corresponding values can be found in Table 1.

The bridging length had a significant impact on the interfragmentary movement. A larger bridging length resulted in a linear increase in relative movement on the near cortex (Fig. 10). A positive linear relationship between bridging length and relative movement was observed on the far cortex.

The objective of the optimization was to minimize the total number of screws. A design with four screws was selected as the optimal design by the evolutionary optimization al-

ration under certain biomechanical constraints. The developed workflow enabled the selection of an optimal screw layout out of several thousand possible arrangements. For this purpose, the finite element mesh generation and the finite element analysis were successfully automated. It is the first procedure which allows for more than the comparison between individual FEAs of different plate osteosynthesis.

The optimization process required minimal user input. The user only needed to segment the bone, position the plate relative to the bone and select a couple of specific points on the model. These points included the material points of bone and plate, the measurement points for the interfragmentary movement as well as the points for force application and constraints. In the future, the user input may be further reduced by an automated segmentation procedure.

The rest of the procedure was performed automatically through a batch file. The selection of an optimal design, based on more than 150 other designs, using an evolutionary algorithm was completed within 24 hours. Further parallelization of the computation process might be able to decrease the computation time.

An improvement to the model might be the integration of more joint and muscle forces in order to make the model more realistic. Integration of a full muscoskeletal model in the simulation model may be achieved using the software AnyBody (AnyBody Technology A/S, Aalborg, Denmark) in the future. This software consists of a detailed model of the femur during gait. It is able to simulate a whole gait and models can be customized, for example the maximum ground reaction force could be adjusted not to exceed 150 N during walking. An interface has already been developed which could map the muscle insertion points from AnyBody's model femur onto the mesh of the individual patient's femur. Since all forces and moments would be in equilibrium, there would be no need to constrain some parts of the model.

Optimal conditions for fracture healing regarding the interfragmentary movement were based on the recommended loading case of 100 N. The overload case was defined with 300 N which is equal to putting around half of the body weight on the injured leg. This value was selected as it represented a considerable increase in force. Furthermore, a much higher force would have probably led to extreme pain for the patient. Another possible extreme scenario could be the simulation of stumbling or even falling.
The integration of anisotropic material properties of bone into a finite element model is challenging and requires high resolution CT data. The alignment of the trabeculae can be used to derive a stiffness tensor which incorporates the anisotropic material properties.

In this work, a bonded interface was selected between bone and defeatured screws. This allowed faster computation. It should be considered that even if the interface has a major influence on the area around the screws, it has almost no influence on the global load deformation behavior such as the interfragmentary movement.

The selected optimum screw arrangement consisted of only four screws. This was the minimum possible number of screws since at least two screws had to be placed in each bone fragment. The selection of a design at the lower end of the design space demonstrated that a minimum number of screws could provide optimal healing conditions. However, the implant construct would fail if only one screw failed. Screws at the distal end of the bone did not affect the simulation outcome and were therefore omitted. However, some surgeons consider them important since they improve the pull-out strength of the screws.

The interfragmentary movement on the near cortex was only 0.22 mm. This movement was considered too small for fracture healing and therefore the selected design cannot be considered "optimal". A constraint which only allows interfragmentary movements larger than 0.3 mm would need to be added to the optimization to avoid insufficient movements. The movement on the far cortex was approximately five times higher compared to the near cortex. This resulted in very different healing conditions on both sides of the bone which may cause non-union. Therefore, the proportion of near cortex movement to far cortex movement should be added as a second objective to the optimization. The healing would be more regular on both sides of the bone with the value being close to 1. An automated workflow has been established, which can be easily adapted for femur geometries from other patients. More patient specific data which also includes osteoporotic bone should be evaluated in order to generate a greater data base. Furthermore, other types of fractures such as diagonal or spiral fractures should be examined. Also a robustness evaluation of the optimal design would be one of the next steps.

Authors // M. Schimmelpfennig (Dynardo GmbH) / C. Wittkowske, S. Raith, J. Jalali, A. Volf, L. Kovacs (Research Group CAPS, TU München) / A. Nolte (CADFEM GmbH), B. König, S. Döbele (Berufsgenossenschaftliche Unfallklinik Tübingen) / J. Bauer, E. Grande Gracia (Institut für diagnostische und interventionelle Radiologie der TU München)

Source // www.dynardo.de/en/library

ANNUAL WEIMAR OPTIMIZATION AND STOCHASTIC DAYS

Your conference for CAE-based parametric optimization, stochastic analysis and Robust Design Optimization in virtual product development.

The annual conference aims at promoting successful applications of parametric optimization and CAE-based stochastic analysis in virtual product design. The conference offers focused information and training in practical seminars and interdisciplinary lectures. Users can talk about their experiences in parametric optimization, service providers present their new developments and scientific research institutions inform about state-of-the-art RDO methodology.

Take the opportunity for an exchange of knowledge with recognized experts from science and industry.

You will find more information and current dates at: **www.dynardo.de/en/wosd**.

We are looking forward to welcoming you to the next Weimar Optimization and Stochastic Days.

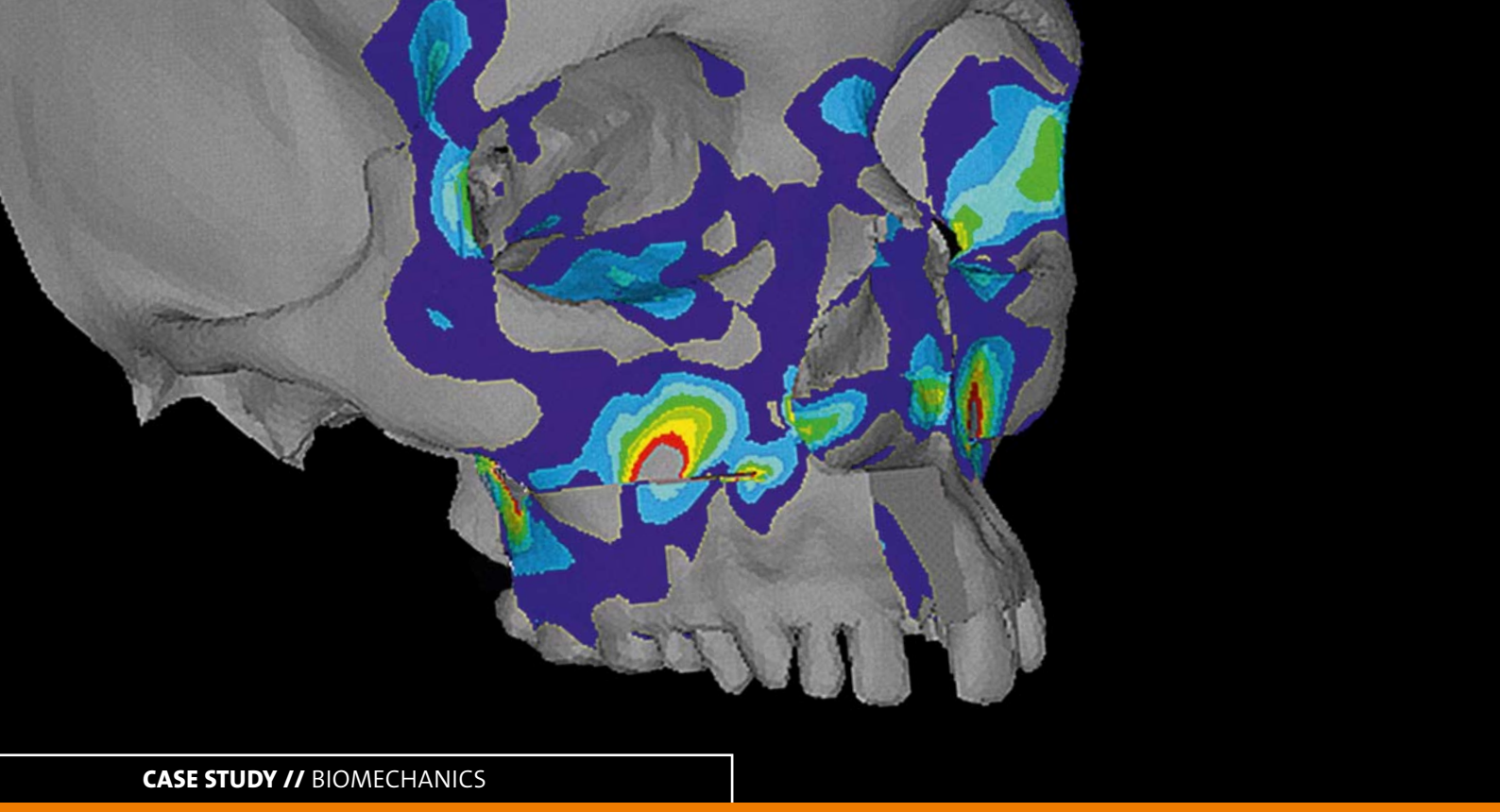

OPTIMIZATION IN MODEL-BASED SIMULATIONS OF SURGICAL PROCEDURES

Optimization of specific data which is based on 3D - finite element analysis is a new method to improve the quality of therapy and enables a fully customized cranial and maxillofacial surgery in a minimal invasive way.

Introduction

Transversal compression and maxillary hypoplasia in adults is seen in nonsyndromal and syndromal patients. In skeletally matured patients the uni- or bilateral transversal compression can be corrected by means of a surgically assisted rapid maxillary expansion (SARME). The treatment is a combination of orthodontics and surgical procedures and provides dental arch space for alignment of teeth. The procedure also causes a substantial enlargement of the maxillary bone base and of the palatal vault. The free space is needed mainly in the middle, so in cases with bilateral transversal compression of the maxilla. In unilateral compression or hypoplasia must be increased predominantly a jaw half.

Distraction osteogenesis is a treatment often used in orthopedics and plastic surgery, but more frequently in maxillofacial surgery. There is a variety of distractors available for use on the different parts of the maxillofacial skeleton.
Since early in the 20th century various techniques have been developed for SARME. The main considerations have opposing interests. One side is a more invasive technique with maximal mobility of the maxillary halves for correction over larger distances with less force but with more possible complications The other side is less invasive with less possible complications but with more relapse, more periodontal problems, and unexpected fractures (Holberg et al. 2007).
The midpalatal suture is historically considered the major place of resistance but this was proven to be untrue by Isaacson and Ingram 1964, Isaacson et al. in 1964 and Kennedy et al. in 1976. A disadvantage of the known methods of intraoral distraction is the poor predictability of the result. Vector of distraction and displacement of the bone parts are subjected to many influences. Some of these factors are known as insertion of distraction force, force application and type of osteotomy. Other influencing factors are largely unknown, such as the geometry of the bone, thickness and density of the bone or soft tissue influences.

A wide variety of techniques and methods to correct transverse maxillary hypoplasia is used without underlying scientific basis. Yet another factor might be the tipping of the maxillary segments instead of parallel expansion due to the different position of the dental-borne and bone-borne distractors relative to the ‘center of resistance’ (Brown et al. 2000, Pinto et al. 2001). This ‘center of resistance’ is a combination

of the area where the maxillary halves are still connected to the skull after the corticotomy, the pterygoid region, and the resistance of the surrounding soft tissues. An exact control of intraoral distraction is need.

Methods

A 21 years old man with a bilateral transversal compression of the maxilla and frontal open bite was treated with a combination of orthodontics and SARME. The dental arch in the anterior region is pointed and not round. The dental arch in the rear region is too narrow for the lower jaw. In figure 1 the plaster model demonstrates the dental position with a tipping of the maxilla, dental rotations and a narrow dental arch. Preoperatively we performed an FEA analysis of the bone model. Therefore we prepared the Dicom data from the CT scan of the scull with mimics software from Materialise company. The final result was a segmented solid model of the maxilla, midface and scull base (figure 2).

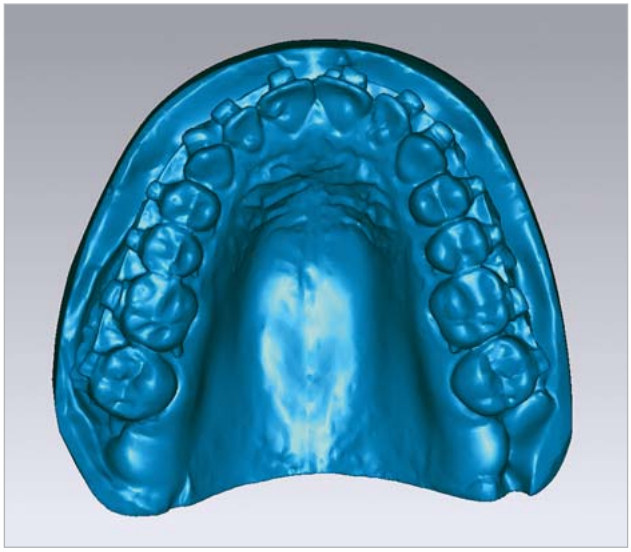

Fig. 1: Plaster model of the maxilla

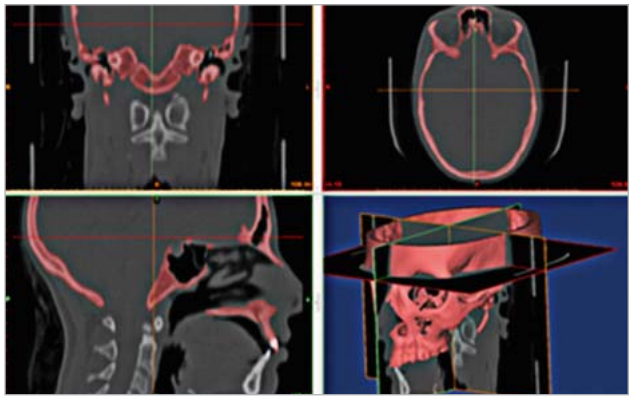

Fig. 2: Segmentation of dicom data

The difference in bone geometry and structure can be represented in a cut in the Le-Fort-I plan, a midfacial plan above the root of the teeth from the cavum nasi straight to the basal pterygoid bone. In figure 3 a cut on the Le-Fort-I plane shows a lot of differences of bone structure on the both sides of the midface. The distribution of the bone structures is quit asymmetric. That means also differences and asymmetries in biomechanical response in case of symmetric bone cut and load.

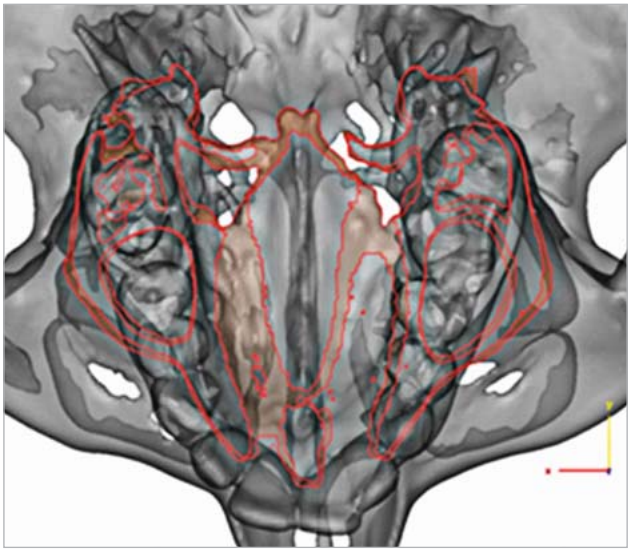

Fig. 3: Asymmetric bone structure in the Le-Fort-I plane

In the next step we inserted fix defined cuts into the segmented model. The scientific literature described a lot of types of osteotomy and modifications. But the indications and the extension of individual osteotomy are not clearly defined. So the disconnecting of the midpalatal suture and the pterygo-maxillary junction is largely fixing.

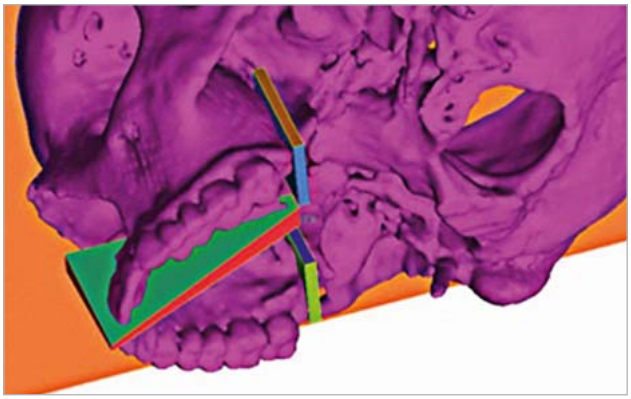

Fig. 4: Fix lines of osteotomy

The osteotomy of the lateral sinus wall is not need in every single case and in full extension. So the extension differs and is determined by the kind of osteotomy. In these areas along the Le-Fort-I plane we defined two cutting areas on each side. We defined an individual start point and an end point on the model of each line of osteotomy. A FEA analysis with ANSYS 14.0 simulates the distraction. For the biomechanical constants we take standard values. The values for reac-

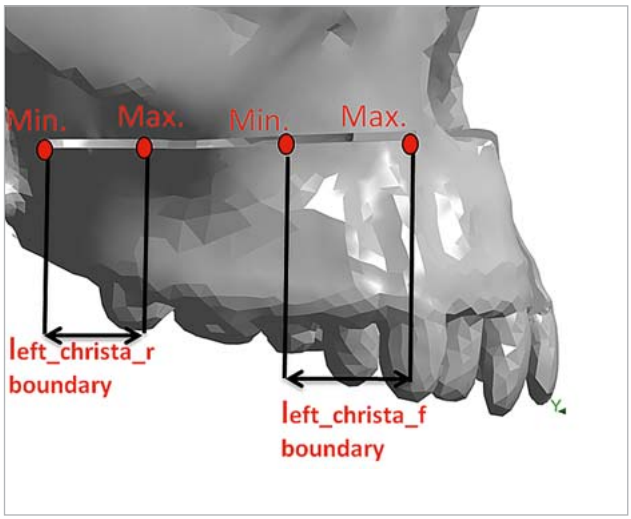

Fig. 5: Individual model based cutting area on right Le-Fort-I plane

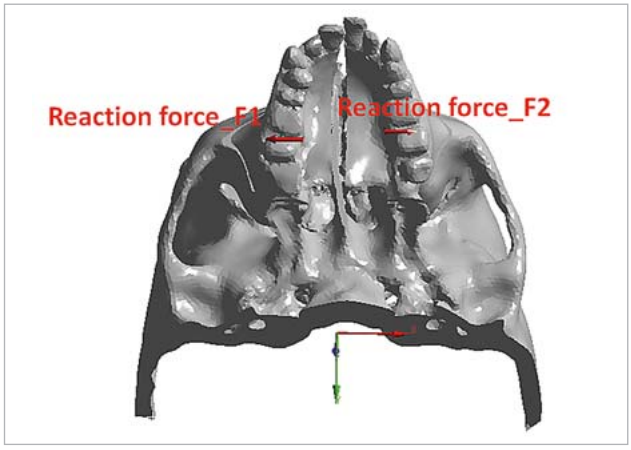

Fig. 6: Reaction forces on the maxilla model

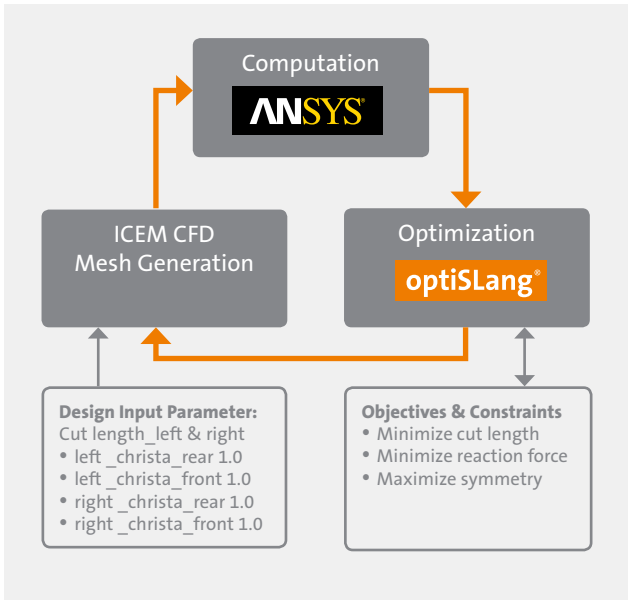

Fig. 7: Optimization workflow

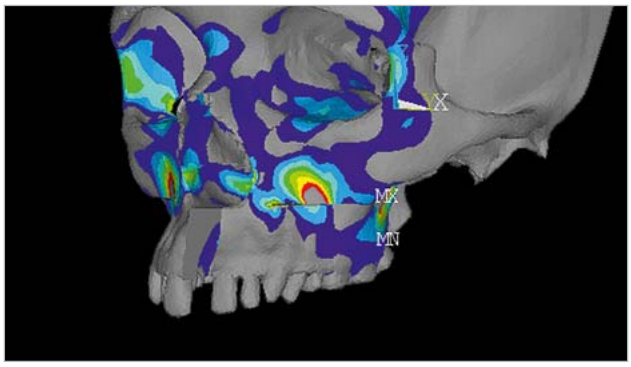

Fig. 8: Finite element analysis of the model after insertion of the fix and individual model based bone cuts

tion forces and fragment moving as well as start points and end points of the lines of osteotomy are input parameters for the optimization routine with optiSLang.

As objectives we defined a maximum of symmetry, a minimum of reaction forces and a minimum of the cutting length. Based on the calculated objective parameters, new start values are set by optiSLang for the cuts and a new iteration loop is started. These parameters inside ANSYS software generate new start values for the cutting areas on both sides. So, a new iteration starts.

Routinely we do about 150 cycles for iteration and pick out these cases with optimal objective parameters. The decision to use a specific result for the operative procedure is exclusively taken by the surgeon. He makes his decision based on his knowledge, skills and experience. Thus, the preoperative analytical workflow serves biomechanically possible cuts on the bone with the greatest possible symmetry, small reaction forces and minimal osteotomy. We transferred the data to an individual template that represents a cutting guide for intraoperative use.

Results

The distribution of the von Mises stresses depends on the anatomical geometry. Higher von Mises stress results from greater expansion values. The results indicate a parallel maxilla widening in transversal direction. Generally high stress levels were observed under the basal plates of distractor. Because of limited elasticity of sphenoid region and complex anatomical geometry high stress level occurs with potentially risk to interferes vascular and neural structures. Low stress level was recognized in dental-alveolar bone. After osteotomy we found an extreme parallel distraction (figure 11). The calculated design was used by the doctor in the surgery. The design of the osteotomy has been transmitted through the mask to the patient. All results were symmetric to a great extent that showed a uniform distraction on each side.

Four weeks after surgery we did a photogrammetric measurement. The mirroring of the face demonstrates almost parallel face. Differences may be due to changes such as hematoma of the soft tissues (figure 12). The exact parallel

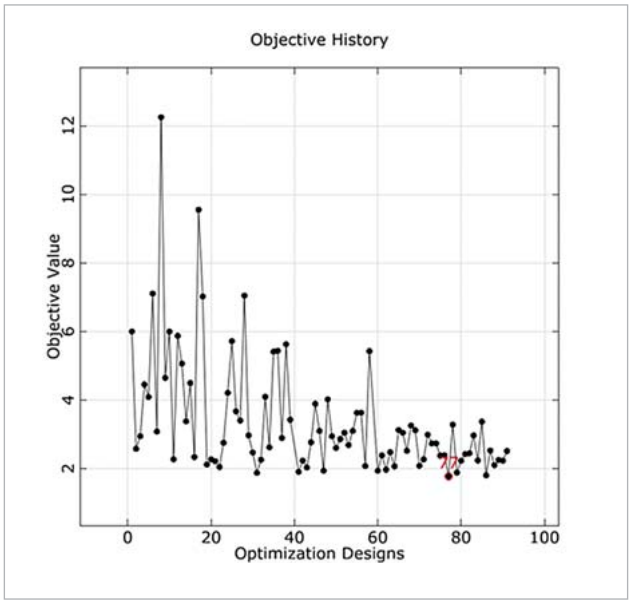

Fig. 9: Optimization process with iteration and objective values

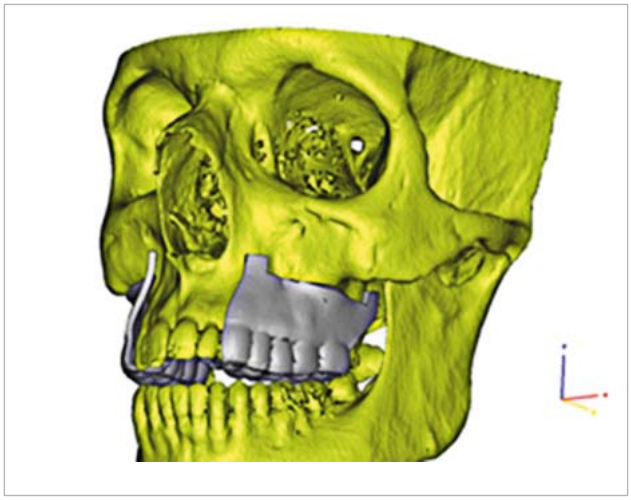

Fig. 10: Cutting guide

Fig. 11: Distraction, after 14 days

distraction of the maxilla is an optimal prerequisite for additionally orthodontic or orthognathic treatment.
The exact parallel distraction of the maxilla is an optimal prerequisite for additionally orthodontic or orthognathic treatment.

Discussion

Standardization in surgical work is important to verify the high quality. Focus on patient's interest, standardization should improve comfort and compliance. Shorter surgical intervention time and better wound healing with reduction of negative side effects are the basis therefore. Minimal invasive surgery under respect of individual anatomical situation is an important way. To evaluate and control stress, strain and forces the FEA with three dimensional analyses of patient's data is valid (Provatidis et al. 2006, Gautam et al. 2007, Provatidis et al. 2007, Boryor et al 2008). Two dimensional methods for evaluation should be replaced by 3D methods. So the future can clear define indication, limitations and contraindications for 3D FEA with optimization strategy. The simulation gives the surgeon only important information. The choice of surgical techniques and the cut is always the responsibility of the physician.

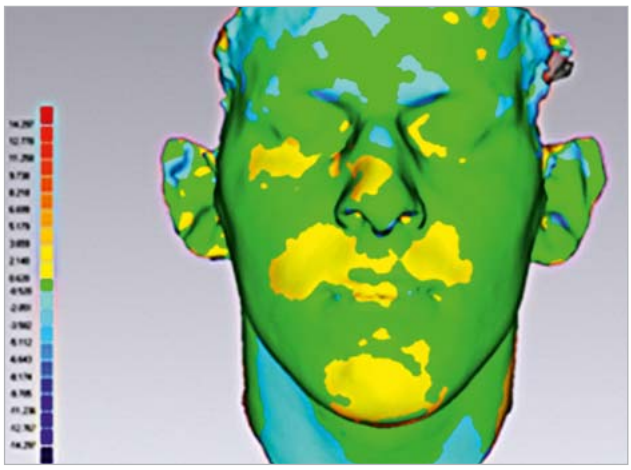

Fig. 12: Comparison of symmetry, 4 weeks after distraction

Conclusion

With 3D analyzing of CT data there is a valid possibility to recognize individual stress distributions in SARME patients using bone anchored distraction device. Extent of osteotomy is individual and depends on stress level of connecting bone structures and the distraction distance. The target parameters (symmetry, low force small cuts) can be obtained with the simulation. The simulation gives important clues for a symmetrical opening of the palate. Analyzing the CT data prior the surgical intervention can help to perform the maxillary bone split in an optimal way with respect to individual anatomic conditions. The finite element model with optimization strategy therefore represents an individual simulation model to evaluate stress and force distribution in maxillary bone structures with optimal conditions for patient specific results.

Authors // Lars Bonitz (Klinikum Dortmund gGmbH, University Witten-Herdecke) / Christoph Mueller (CADFEM GmbH)

Source // www.dynardo.de/en/library

SIMULATION, OPTIMIZATION AND TESTING – SUCCESSFULLY COMBINED

The calculation of the structural and mechanical behavior of electric machines already in the conceptual design phase helps to reduce development cycles and to fulfill the complex demands on the components properties.

In most cases, geometries and components are generated only virtually in the early project phase. This makes the validation of simulations much more complicated. Therefore, robust and physically-based calculation methods are required using the data of standardized material tests. Mechanical material data can generally be obtained from existing data sheets or are generated by analytical calculations and standardized load tests of material samples. This approach reaches its limits if a heterogeneous material structure exists that cannot be resolved practicably with the Finite-Element-Method (FEM).

FEM-compatible material parameters

Here, a process is described which allows a standardized generation of FEM-compatible material parameters of heterogeneous material structures via model updating. The procedure is going to be explained using the example of a resin-impregnated copper windings as part of electrical machines. In this case, model updating means the iterative variation of selected model parameters to obtain an optimal calibration between the results of a simulative and experimental modal analysis.

The copper wires fixed in the stator slots of permanent magnet synchronous machines are embedded in a thermoset matrix for electrical insulation, thermal connectivity as well as mechanical fixation. A detailed resolution of the fine slot structure in structural-mechanical simulations is impractical because of the highly intensive modelling and computation effort. A pragmatic way to overcome that issue is to substitute the heterogeneous material model of the copper windings with a homogeneous one having transversely isotropic properties. The stiffness behavior of the slot structure is described by five independent surrogational parameters.

The quantification of the surrogational parameters is conducted by comparing the ANSYS simulation results of the Eigenfrequencies and deflection shapes of a specimen with the results of an experimental modal analysis. A section of the copper windings of an electric machine stator (Fig. 2) was used as a test specimen.

Optimization of the surrogational parameters

For the experimental modal analysis a laser scanning vibrometer was used to measure the surface velocities in

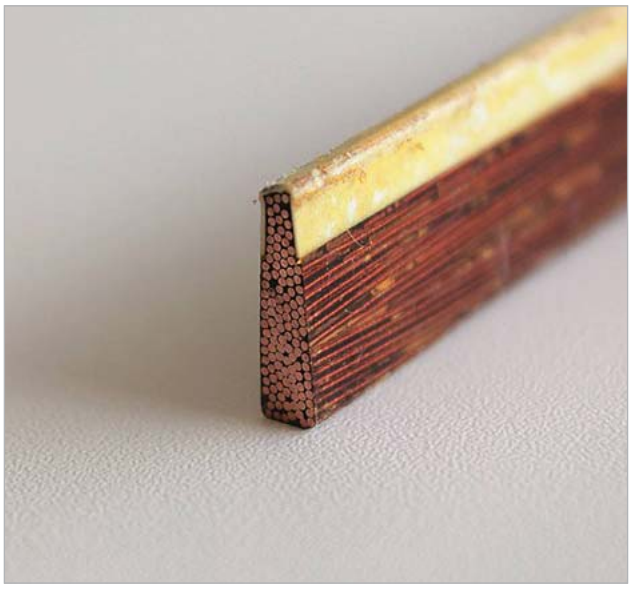

Fig. 2: View of the specimen made of copper windings embedded in a resin matrix

normal direction to the longitudinal area of the test specimen. In order to provide an appropriate design space for the model updating, the classical laminate theory by Chamis was used. Because of the analytical correlations, it is possible to calculate the surrogational parameters for the simulation of a transversely isotropic material by using the properties of the base material - in this case, copper and resin. The design space can be set symmetrically around the analytically calculated base values.

The model updating for the identification of the surrogational material parameters is performed automatically in optiSLang. The objective function of the optimization task consists of terms which compare the modal deflection shapes using the Modal Assurance Criterion (MAC), as well as terms which take into account the variation of the Eigenfrequencies.

In Figure 3 (top), the experimentally identified Eigenfrequencies and deflection shapes of the sample up to 6 kHz are shown. Within the first and fourth bending moment in the longitudinal direction of the structure, the slightly conical cross-section of the sample causes, in some modes, an antiphase vibration over the width of the sample (see Figure 3, right). The simulation, based on the analytically calculated surrogational parameters, shows nine Eigenfrequencies in the same frequency spectrum. A sensitivity analysis of the five orthotropic surrogational parameter showed a strong correlation between the objective function and the modulus of elasticity in fiber direction as well as a lower correlation between the objective function and the shear modulus in opposite fiber direction. The variation of the other parameters neither affected significantly the Eigenfrequencies nor the mode shapes.

According to the response shape (Fig. 4), both modulus of elasticity in fiber direction and shear modulus in opposite fiber direction can be optimized in regard to the objective

Fig. 3: Comparison of the experimental (top) and simulated mode shapes

function. Due to the low significance, the values for the Poisson's ratios of the system as well as for the modulus of elasticity in opposite fiber direction can be equated with the analytically calculated values.

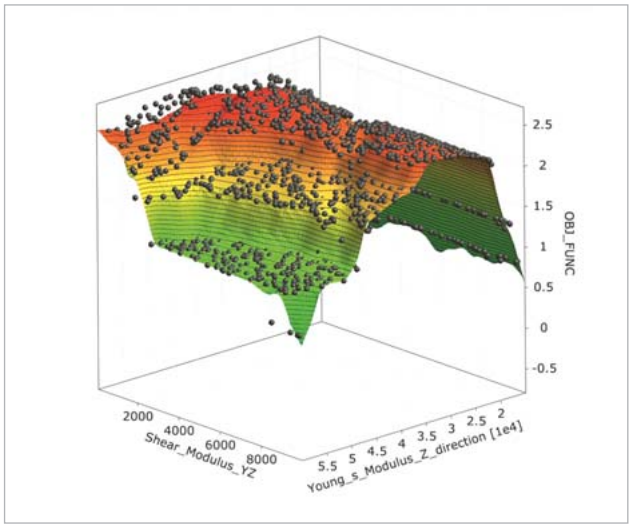

Fig. 4: Response shape for the parameters of the elasticity modulus in fiber direction and shear modulus opposite fiber direction in regard to the optimization criterion

The deviation of Eigenfrequency was reduced

When comparing the MAC-matrix calculated by using the obtained material data to the MAC-matrix derived from the analytically calculated material data, a significant improvement of the MAC-values of all compared modes can be seen. The MAC-value of the 2nd mode shape could be increased by 20%, the one of the 4th mode shape was even doubled by the optimization. At the same time, the Eigenfrequency deviation between experiment and simulation could be reduced for all modes. The non-identified modes of the experimental modal analysis were either not sufficiently stimulated (eg. torsional vibrations) or not directed normally to the longitudinal surface of the specimen (eg. bending mode in transverse direction).

Altogether, the automated model updating quickly generated a set of FEM-compatible surrogational material data representing the structural dynamic behavior of the copper windings for a transversely isotropic modeling approach. With this process, concepts can be evaluated significantly more accurately regarding their mechanical properties in early project phases. There is also the opportunity to further analyze and understand even hardly quantifiable model parameters - such as contact stiffness or temperature induced residual stress. In summary, this can be seen as an important step towards a higher correspondation between simulation and experiment.

Authors // M. Schwarzer, Dr.-Ing. E. Barti (BMW Group) / Prof. Dr.-Ing. Th. Bein (Fraunhofer LBF Darmstadt)

Source // www.dynardo.de/en/library

METHOD OVERVIEW

Process automation and process integration
- Workflow definition via graphical user interface
- Reliable use with help of wizards
- Robust default settings for all algorithms
- Connection of arbitrary complex process chains
- Generate and use templates of process chains
- Parallelization and distribution of design evaluation
- Direct integration of Matlab, MS Excel, Python and SimulationX
- Supported connection of ANSYS, Abaqus, Adams, MADYMO
- Arbitrary connection of ASCII file interfaced solvers
- Full integration of optiSLang in ANSYS workbench
- Python interfaces to optiSLang algorithmic library
- Automatic generation and adaption of user flows via python scripting

Sensitivity analysis
- Classical Design of Experiments
- Advanced Latin Hypercube Sampling
- Correlation coefficients (linear, quadratic, rank-order)
- Principal Component Analysis
- Polynomial based Coefficient of Determination
- Polynomial based Coefficient of Importance
- Metamodel of Optimal Prognosis (MOP) with Coefficient of Prognosis (CoP)
- MOP/CoP based sensitivity indices for important variables

Multidisciplinary nonlinear optimization
- Continuous, discrete and binary design variables
- Gradient based optimization (NLPQL)
- Global Response Surface optimization using MOP with best design validation
- Adaptive Response Surface Method
- Evolutionary Algorithms (EA)
- Particle Swarm Optimization (PSO)
- Stochastic Design Improvement
- Multiobjective optimization using weighted objectives
- Multiobjective Pareto optimization with EA and PSO
- Start design import from previous samples

Parameter identification
- Parametrization and monitoring of response signals
- Signal function library including FFT, filtering etc.
- Sensitivity analysis using MOP/CoP to check identifiability
- Flexible definition of identification goal functions
- Local and global optimization methods to search for optimal parameters

Robustness evaluation
- Continuous and discrete random variables
- More then 20 probability distribution functions
- Distribution fits using measurements
- Correlated input variables using the Nataf model
- Monte Carlo and Advanced Latin Hypercube Sampling
- Statistical assessment of output variation including:
  - histograms with automated distribution fits
  - stochastic moments
  - quantile and sigma level estimation
- Sensitivity analysis with respect to random variables using correlations and MOP/CoP

Reliability analysis
- Definition of arbitrary limit states
- Monte Carlo and Latin Hypercube Sampling
- First Order Reliability Method (FORM)
- Importance Sampling Using Design Point (ISPUD)
- Directional Sampling
- Asymptotic Sampling
- Adaptive Response Surface Method

Robust Design Optimization (RDO)
- Sequential and fully coupled procedures
- Variance based RDO
- Reliability based RDO
- Flexible definition of robustness measures using e.g. mean values, variances, Taguchi loss functions and probability of failure
- Consideration of robustness measures in optimization constraints and objectives functions

Post processing
- Statistic post processing including anthill plots, correlation plots and sensitivity indices
- Approximation post processing including 2D and 3D plots of response surfaces and the MOP
- Optimization post processing including Pareto frontier and convergence history of design variables, responses, objectives and constraints
- Show solver output images
- Parallel coordinates plot
- Traffic light plot
- Full interaction of single plots
- Design classification using coloring, selection/deselection
- High quality outputs in BMP, PNG, SVG, EPS and PDF format

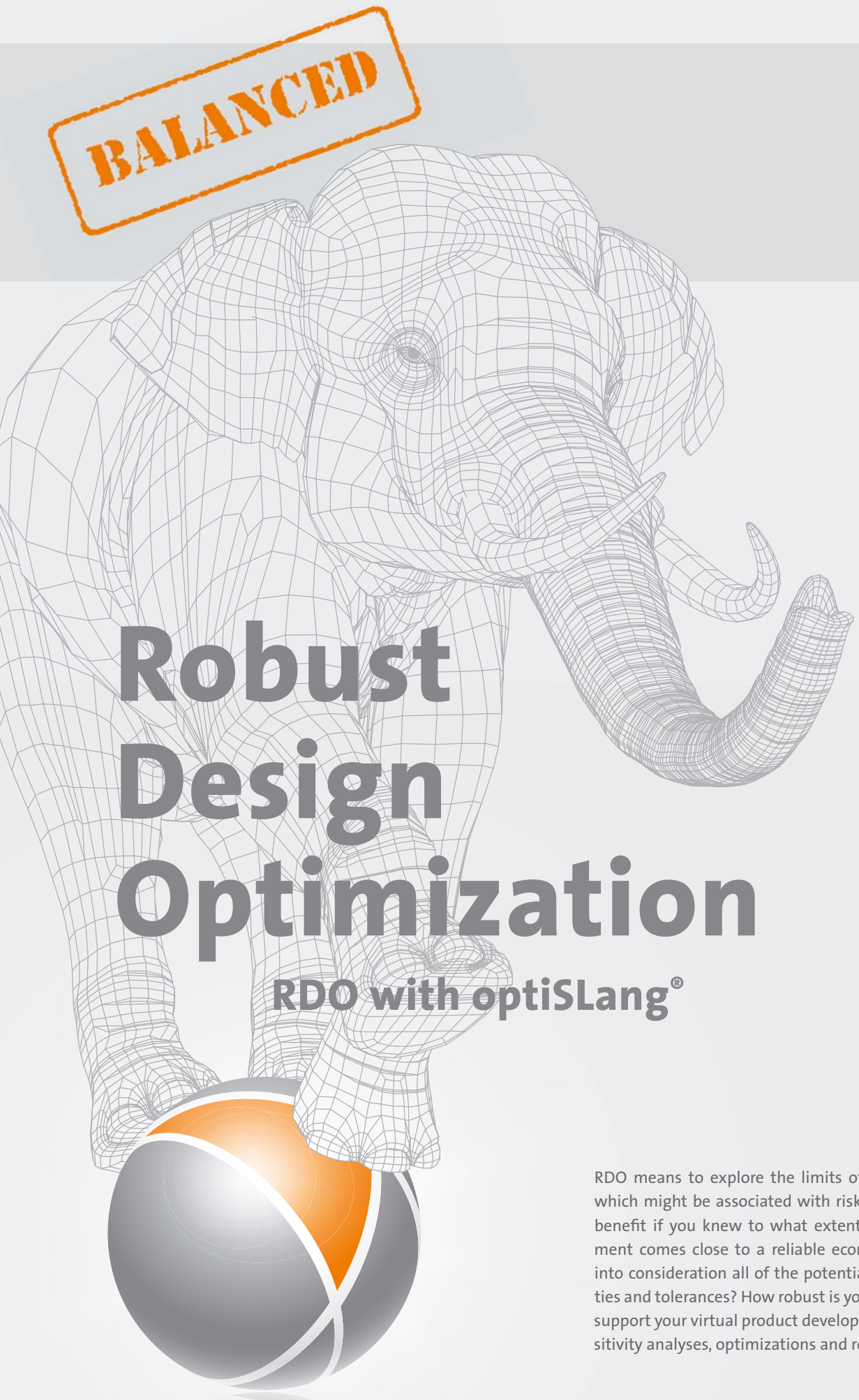

Robust Design Optimization

RDO with optiSLang®

RDO means to explore the limits of product performance, which might be associated with risks. What would be your benefit if you knew to what extent your product development comes close to a reliable economic optimum taking into consideration all of the potentially affecting uncertainties and tolerances? How robust is your design in reality? We support your virtual product development with efficient sensitivity analyses, optimizations and robustness evaluations.

CONSULTING, SUPPORT, TRAININGS

Dynardo's consulting team has extensive expertise in the application of CAE-based analysis and Robust Design Optimization in the fields of structural mechanics and dynamics. At seminars and events, we provide basic or expert knowledge of our software products and inform you about methods and current issues in the CAE sector.





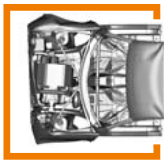

CAE-Consulting

The Dynardo GmbH offers customized calculation and simulation services in various fields of industries, e.g. consumer goods industry, mechanical and process engineering, energy industry, civil engineering, geomechanics, automotive industry, aerospace industry, biomechanics and micromechanics. We give support in all phases of product development: from the first predevelopment and feasibility studies over sensitivity analysis up to the development of the optimal design by robustness evaluation and reliability analysis. Due to the company's combination of software development and consulting, we achieve a high amount of flexibility referring to special market requirements in the CAE sector.

Support

The main interest of our support team is a successful customer. We provide technical support by phone, e-mail or online. All requests regarding our software products optiSLang, multiPlas, SoS and ETK will be processed thoroughly and answered immediately. Our support team will also help you to implement efficient RDO applications and its various methods to solve CAE-challenges in your particular field of business.

Information Days and Webinars

During our info days and webinars, you will receive an introduction to performing complex, non-linear FE-calculations using optiSLang, multiPlas, SoS and ETK. At regular webinars, you can easily get information about all relevant issues of CAE-based optimization and stochastic analysis. During an information day, you will additionally have the opportunity to discuss your specific optimization task with our experts and develop first approaches to solutions.

Trainings

For a competent and customized introduction to our software products, visit our basic or expert trainings clearly explaining theory and application of a sensitivity analysis, multidisciplinary optimization and robustness evaluation. The trainings are not only for engineers, but are also perfectly suited for decision makers in the CAE-based simulation field. For all trainings there is a discount of 50% for students and 30% for university members/PHDs. You can find an overview of the current training program at our homepage www.dynardo.de.

Internet Library

Our internet library is the perfect source for your research on CAE-topics and applications of CAE-based RDO. There you will find practical references and state-of-the-art case studies matched to the different fields of methods and applications.

Infos

www.dynardo.de/en/consulting
www.dynardo.de/en/trainings
www.dynardo.de/en/library

Contact & Distributors

Germany & worldwide

Dynardo GmbH
Steubenstraße 25
99423 Weimar
Phone: +49 (0)3643 9008-30
Fax.: +49 (0)3643 9008-39
www.dynardo.de
contact@dynardo.de

Dynardo Austria GmbH
Office Vienna
Wagenseilgasse 14
1120 Vienna
www.dynardo.at
contact@dynardo.at

Germany

CADFEM GmbH
Marktplatz 2
85567 Grafing b. München
www.cadfem.de

science + computing ag
Hagellocher Weg 73
72070 Tübingen
www.science-computing.de

Austria
CADFEM (Austria) GmbH
Wagenseilgasse 14
1120 Wien
www.cadfem.at

Switzerland
CADFEM (Suisse) AG
Wittenwilerstrasse 25
8355 Aadorf
www.cadfem.ch

Czech Republic, Slovakia, Hungary
SVS FEM s.r.o.
Škrochova 3886/42
615 00 Brno-Židenice
www.svsfem.cz

Sweden, Denmark, Finland, Norway
EDR & Medeso AB
Lysgränd 1
SE-721 30 Västerås
www.medeso.se

United Kingdom of Great Britain and Northern Ireland
IDAC Ltd
Airport House Business Centre
Purley Way
Croydon, Surrey, CR0 0XZ
www.idac.co.uk

Ireland
CADFEM Ireland Ltd
18 Windsor Place
Lower Pembroke Street
Dublin 2
www.cadfemireland.com

Turkey
FIGES A.S.
Teknopark Istanbul
Teknopark Bulvari 1 / 5A-101-102
34912 Pendik-Istanbul
www.figes.com.tr

North Africa
CADFEM Afrique du Nord s.a.r.l.
Technopôle de Sousse
TUN-4002 Sousse
www.cadfem-an.com

Russia
CADFEM CIS
Suzdalskaya 46, Office 203
111672 Moscow
www.cadfem-cis.ru

India
CADFEM Engineering Services India
6-3-902/A, 2nd Floor, Right Wing
Rajbhawan Road, Somajiguda
Hyderabad 500 082
www.cadfem.in

USA

CADFEM Americas, Inc.
27600 Farmington Road, Suite 203 B
Farmington Hills, MI 48334
www.cadfem-americas.com

Ozen Engineering Inc.
1210 E Arques Ave 207
Sunnyvale, CA 94085
www.ozeninc.com

USA/Canada
SimuTech Group Inc.
1800 Brighton Henrietta Town Line Rd.
Rochester, NY 14623
www.simutechgroup.com

Japan
TECOSIM Japan Limited
4F Mimura K2 Bldg. 1-10-17
Kami-kizaki, Urawa-ku, Saitama-shi
Saitama 330-0071
www.tecosim.co.jp

Korea
TaeSung S&E Inc.
Kolon Digital Tower 2
10F, Seongsu-dong 2 ga
Seongdong-gu
Seoul 333-140
www.tsne.co.kr

China
PERA-CADFEM Consulting Inc.
Bldg CN08, LEGEND-TOWN
Advanced Business Park,
No. 1 BalizhuangDongli,
Chaoyang District,
Beijing 100025
www.peraglobal.com

Imprint

Publisher
Dynardo GmbH
Steubenstraße 25
99423 Weimar
www.dynardo.de
contact@dynardo.de

Executive Editor & Layout
Henning Schwarz
henning.schwarz@dynardo.de

Registration
Local court Jena: HRB 111784

VAT Registration Number
DE 214626029

Publication
worldwide

© Images
Fotolia: p. 6-photosoup
BMW Group: p. 28-29